# MEJS

## MIDDLE EAST JOURNAL OF SCIENCE

CONTENTS

# INVESTIGATION OF TEMPERATURE DEPENDENCE OF D₂O SOLUTIONS BY 400 MHZ NMR

*Canan Aytuğ Ava[1], Gülten Kavak Balcı\*[1], Ali Yılmaz[2]*

[1]Dicle University, Department of Physics, Diyarbakir, 21280 TURKEY

[2]Batman University, Department of Physics, Batman, 72060 TURKEY

\* Corresponding author; gulten@dicle.edu.tr

**Abstract:** *The rate of water proton relaxation of protein solutions were studied in the presence and absence of the paramagnetic ions [gadolinium (III), manganese (II), chromium (III), iron (III), nickel (II), copper (II), and cobalt (II)]   in the previous studies. However, these studies were carried out rather at low frequencies. Therefore, studying of temperature dependence of relaxation rates for absence and presence of 2 % albumin in pure $D_2O$ by 400 MHz will be a novelty.*

*In this study, $T_1$ and $T_2$ relaxation ratios of $D_2O$ and $0.1 H_2O/0.9D_2O$ solutions were investigated with respect to temperature for pure and  for constant  albumin  concentration(2%). The experiments were carried out by using Bruker Avance 400 MHz NMR. Inversion Recovery (180-τ-90) pulse step were used for $T_1$, whereas Carr-Purcell-Meiboom-Gill pulse step were used for $T_2$.  The experiments were performed for temperature range of 20°C-40°C by using automatic temperature control unit.*

*$1/T_1$ and $1/T_2$ decrease linearly with increasing temperature for pure $D_2O$ solutions. However, for $0.1H_2O/0.9D_2O$ solutions, the relaxation rates of $T_1$ increase with increasing temperature while $T_2$ decreases with increasing temperature. The decrease in both relaxation rates of the $D_2O$ solution with respect to the increased temperature suggests that relaxation is due to spin relaxation interaction. Increasing of relaxation rates with the increasing temperature, in the presence of albumin demonstrates the validity of the dipolar mechanism*

Keywords: *NMR, $T_1$, $T_2$, relaxation, albumin, manganese (Mn)*

## 1. Introduction

Human serum albumin (HSA) is the most abundant serum protein in plasma and has a high ligand binding capacity that can bind a wide variety of compounds. HSA contributes to various physiological functions such as homeostasis, metabolism, protection, and also the passage and binding of endo-exogenous substrates [1, 2, 3]. Spin-lattice ($T_1$) and spin-spin ($T_2$) relaxation times of albumin solutions were studied in detail by Nuclear Magnetic Resonance Dispersion (NMRD) and Nuclear Magnetic Resonance (NMR) techniques [4-21]. Several methods have been applied to explain the mechanisms of the reaction. One of these methods is based on the derivation of albumin's rotational correlation (interest) time from the Stokes-Einstein association [8, 13, 16, 17]. The other is based on

the time of interest obtained from $T_1/T_2$ ratios [21, 22]. The interest times in microseconds in the first studies are derived from nanoseconds in subsequent studies. The difference is explained by the high protein concentration (such as 10% or 15%) used in the initial studies.

The development of contrast agents to bind a ligand to HSA has a central value in view of displaying vessels with abnormal vascular permeability [23, 24]. For this reason, studies on albumin solutions containing paramagnetic centers are still valuable. The albumin solutions containing manganese were investigated by many people [20, 25 –29]. However, the effect of the manganese found in albumin $D_2O$ solutions on $T_1$ and $T_2$ relaxation has not yet been investigated at 400 MHz. In this study, $T_1$ and $T_2$ of $D_2O$ solutions containing various ion concentrations were investigated in NMR. The same ion concentrations were then examined in terms of the effects of $T_1$ and $T_2$ in the presence of 0.02 g of albumin. In addition, measurements were made by varying protein concentrations for specific ion concentrations.

## 2. Materials and Methods

**Preparation of Stock solutions -** A stock solution was prepared by adding 0.003 g of $MnCl_2$ in 20 ml of $D_2O$. The prepared stock solution was thoroughly shaken and the mouth part was completely closed with parafilm to prevent air ingress. 20 μl of this solution contains 1 μg Mn (II).

**Temperature measurements were carry out for the following solutions ;-** The temperature-dependent change of ion-containing $D_2O$ solution was investigated for sample prepared by taking 40 μl of the stock solution and 960 μl of $D_2O$. The temperature dependence of this solution was also investigated by adding 0.02 g of albumin.

**NMR Measurements-** NMR $T_1$ and $T_2$ relaxation times measurements of the prepared samples were made at 20⁰ C, 25⁰ C, 30⁰ C, 35⁰ C and 40⁰ C. Temperatures were changed with the help of automatic temperature control system. Relaxation time measurements were performed with the BRUKER-Avance 400 MHz NMR spectrometer. $T_1$ and $T_2$ relaxation times were performed by using Inversion Recovery and Carr-Purcell-Meiboom-Gill pulse steps, respectively. Pulse repetition time was taken as $5T_1$ for $T_1$ measurements. Inversion Recovery and Spin Echo delay times were changed in accordance with relaxation recovery and decay processes.

## 3. Results and Discussion

In this study, we presented measured $T_1$ and $T_2$ relaxation times of HSA solutions at temperatures 20–45 ⁰ C.  $1/T_1$ and $1/T_2$ relaxation ratios were investigated with respect to temperature for pure and for constant albumin concentration (2%).  The value of the measurements were summarized in Table 1. and 2. We plotted $T_1$ and $T_2$ relaxation rates versus $T$ in order to understand the influence of temperature. Graphs are shown in Figure 1.

Table 1. The Spin-lattice relaxation rates ($1/T_1$) of albumin and albumin free solutions as a function of temperature ($T$)

| Temperature (K) | 0.02g alb+$D_2O$ $1/T_1(s^{-1})$ | pure $D_2O$ $1/T_1(s^{-1})$ |
|---|---|---|
| 293 | 1.592 | 1.197 |
| 298 | 1.6 | 1.075 |
| 303 | 1.63 | 0.946 |
| 308 | 1.65 | 0.846 |
| 313 | 1.66 | 0.767 |

Table 2. The spin-spin relaxation rates ($1/T_2$) of albumin and albumin free solutions as a function of temperature ($T$)

| Temperature(K) | 0.02 g alb+ $D_2O$  $1/T_2 (s^{-1})$ | pure $D_2O$ $1/T_2 (s^{-1})$ |
|---|---|---|
| 293 | 26.52 | 46.14 |
| 298 | 23.64 | 41.89 |
| 303 | 20.32 | 38.87 |
| 308 | 18.11 | 33.3 |
| 313 | 15.87 | 29.1 |
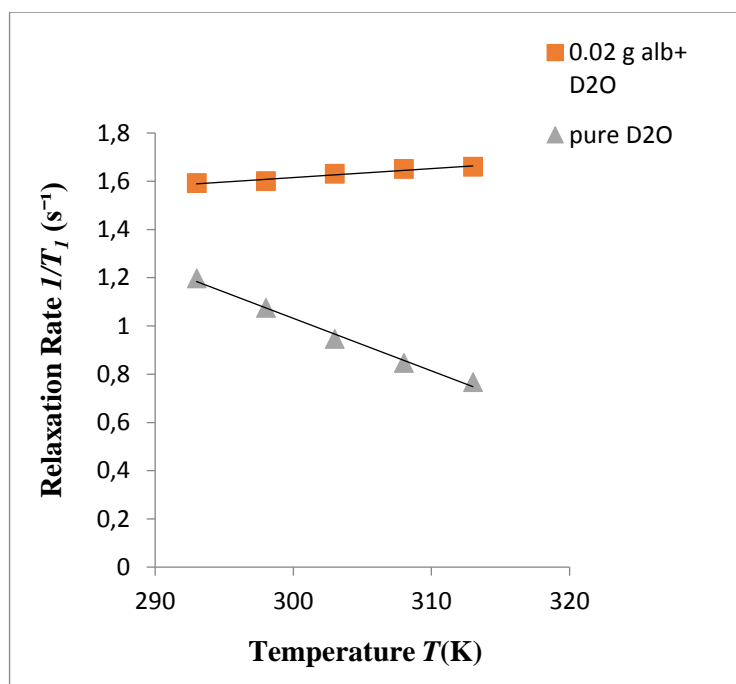
(A)
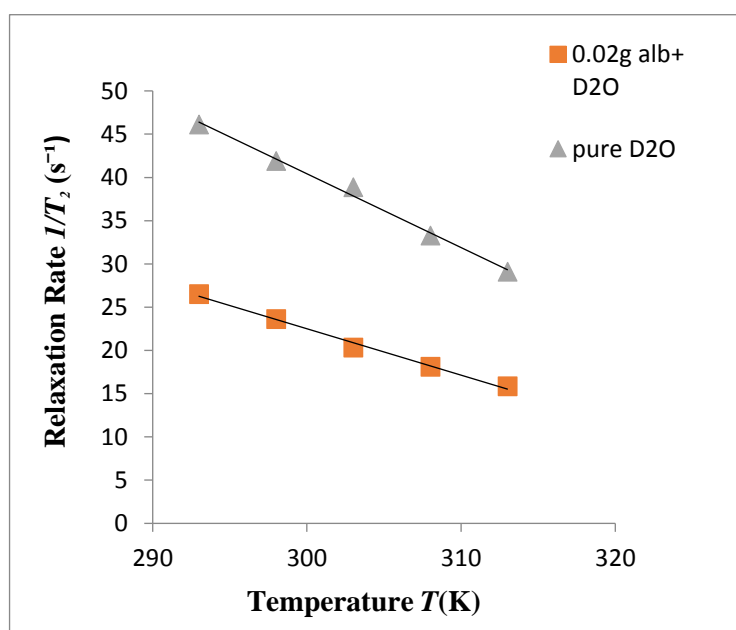


(B)

Figure 1.  Temperature dependence of the spin–lattice ($R_1$) (A) and spin–spin
relaxation rate ($R_2$) (B), for pure and protein-contained $D_2O$ solutions

It can be seen that the change of $1/T_1$ and $1/T_2$ relaxation rates with temperature ($T$) is linear, but in the presence of 0.02 g albumin, the $1/T_1$ ratio of $D_2O$ increases linearly with increasing temperature while decreases linearly in the absence of albumin. In addition, in the presence and

4

absence of 0.02 g albumin, the $1/T_2$ relaxation rate of $D_2O$ decreases linearly with increasing temperature (Fig.1).

Decreasing of the $1/T_1$ and $1/T_2$ values with temperature in $D_2O$ solutions suggests that the dipole-dipole interaction mechanism is predominant [19-21]. In addition, the increase of $1/T_1$ with temperature in the $D_2O$ solutions shows that the mechanism of spin-rotation interaction is predominant. The relaxation rates in all solutions has been found that high correlation for each fit and vary linearly with temperature [22].

**4. Conclusions**

The $1/T_1$ and $1/T_2$ vary linearly with temperature and has a high influence to alter relaxation of solution studied. The least-squares fitting of $1/T_1$ and $1/T_2$ versus $T$ gives a linear relationship, and the data suggest that the relaxation mechanism of HSA is caused by a fast chemical exchange of water molecules between protein-bound water and free water. Decreasing and increasing of the relaxation rates ($1/T_1$ and $1/T_2$) values with increasing temperature in $D_2O$ solutions suggests that the dipole-dipole interaction and spin-rotation interaction mechanism is predominant, respectively.

**References**

[1] Cistola, D.P., Small, D.M., "Fatty acid distribution in systems modeling the normal and   diabetic human circulation. A $^{13}C$ nuclear magnetic resonance study", J. *Clin. Invest*, 87, 1431-1441, 1991.

[2] Fasano, *et al.*, "The extraordinary ligand binding properties of human serum albumin", *IUBMB Life,* 12, 787-796, 2005.

[3] Sulkowska, *et al.*, "The competition of drugs to serum albumin in combination chemotherapy: NMR study", *J. Mol. Struct*. 744, 781-787**,** 2005.

[4] Yilmaz, *et al.,* "NMR proton spin-lattice relaxation mechanism in $D_2O$ solutions of albumin determined at 400 MHz", *Journal of Applied Spectroscopy,* 81**,** 365-370**,** 2014.

[5] Koenig S.H, Schillinger W.E., "Nuclear magnetic relaxation dispersion in protein solutions. I. Apotransferrin". *J Biol Chem.,* 244, 3283-**32**89**,** 1969.

[6] Gösch, L., Noack, F.L., "NMR relaxation investigation of water mobility in aqueous bovine serum albumin solutions", *Biochim. Biophys. Acta***,** 453**,** 218-232**,** 1976.

[7] Hallenga, K., Koenig, S.H., **"**Protein rotational relaxation as studied by solvent $^1H$ and $^2H$ magnetic relaxation", *Biochemistry*, 15, 4255-4264, 1976.

[8] Oakes, J., **"**Protein hydration. Nuclear magnetic resonance relaxation studies of the state of   water in native bovine serum albumin solutions", *J. Chem. Soc. Farad. Trans*., 72, 216-227, 1976.

[9] Gallier, *et al.*, **"**$^1H$- and $^2H$-NMR study of bovine serum albumin solutions", *Biochim. Biophys. Acta.*, 915, 1-18, 1987.

[10] Koenig, S.H., Brown, R.D., **"**A molecular theory of relaxation and magnetization   transfer: Application to cross-linked BSA, a model for tissue", *Magn. Reson. Med.*, 30, 685-695, 1993.

[11] Koenig, *et al*., **"**Magnetization transfer in cross-linked bovine serum albumin solutions at   200 MHz: A model for tissue", *Magn. Reson. Med.,* 29,  311-316, 1993.

[12] Koenig, S.H., **"**Classes of hydration sites at protein-water interfaces: The source of contrast in magnetic resonance imaging", *Biophys. J*., 69, 593-603, 1995.

[13] Bryant, R.G., **"**The dynamics of water protein interactions", *Ann. Rev. Biophys. Biomol. Struct.,* 25, 29-53, 1996.

[14] Denisov, *et al.*, **"**Using buried water molecules to explore the energy landscape      of    proteins", *Nat. Struct. Biol.*, 3, 505–509, 1996.

[15] Bertini, *et al*., **"**^{1}H NMRD profiles of diamagnetic proteins: a model-free analysis", *Magn. Reson. Chem.*, 38, 543-550, 2000.

[16] Kiihne, S., Bryant, R.G., **"**Protein-bound water molecule counting by resolution of [1]H       spin-lattice relaxation mechanisms", *Biophys. J*., 78, 2163-2169, 2000.

[17] Denisov, V.P., Halle, B., **"**Hydrogen exchange rates in proteins from water ^{1}H transverse magnetic relaxation", *J Am. Chem. Soc*., 124, 10264-10265, 2002.

[18] Van-Quynh, *et al*., **"**Protein reorientation and bound water molecules     measured by ^{1}H magnetic spin-lattice relaxation", *Biophys. J*., 84, 558-563, 2003.

[19] Halle, B., **"**Protein hydration dynamics in solution: a critical survey", Philos. T. Roy. *Soc.   Lond. B*., 359, 1207-1224, 2004.

[20] Bertini, *et al.,*  **"**NMR Spectroscopic detection of protein protons and longitudinal relaxation rates between 0.01 and 50 MHz", *Angew. Chem.*, 117, 2263-2265, 2005.

[21] Yilmaz, *et al.*, **"**Determination of the effective correlation time modulating 1H NMR relaxation processes of bound water in protein solutions", *Magn. Reson. Imaging*, 26, 254-260, 2008.

[22] Yilmaz, A., Zengin, B., **"**High-field NMR T(2) relaxation mechanism in D2O solutions of albumin",  *Journal of Applied Spectroscopy*, 80,  335-340, 2013.

[23] Kang, M.S., *et al*., "Isolation of chitin synthetase from Saccharomyces cerevisiae.  Purification of an enzyme by entrapment in the reaction product". *J Biol Chem.,* 259, 14966-14972, 1984.

[24] Elst, *et al.,* **"**Subtle prefrontal neuropathology in a pilot magnetic resonance spectroscopy study in patients with borderline"*, J Neuropsychiatry Clin Neurosci*, 13, 511–514. 2001.

[25] Barnhart, J.L., Berk, R.N., **"**Influence of paramagnetic ions and pH on proton NMR relaxation of biologic fluids"*, Invest radiol.,* 21, 132-136, 1986.

[26] Silvio, *et al*., **"**[1]H and [17]O  relaxometric investigations of the binding of Mn(II) ion to human serum albumin", *Magnetic Resonance in Chemistry,* 40, 41-48, 2002,

[27] Korb, J.P, Bryant, R.G., "Magnetic field dependence of proton spin-lattice relaxation times", *Magnetic Resonance in Medicine*, 48, 21-26, 2002.

[28] Kruk, D., Kowalewski, J., **"**Nuclear spin relaxation in paramagnetic systems (S>/=1) under fast rotation conditions", *J Magn. Reson.*, 16, 229-40, 2003.

[29] Yılmaz, *et al.,*  "Observation of Triplet traces obtained with inversion recovery method in  both residual water- and H2O/D2O-albumin mixture by using 400 MHz proton NMR, *Asian Journal of Chemistry*, 25**,** 2104-2108**,** 2013.

# AB-INITIO CALCULATIONS OF STRUCTURAL, ELECTRONIC AND MAGNETIC PROPERTIES OF LiRh₂Si₂

*Gülten Kavak Balcı\*¹, Seyfettin Ayhan¹*

¹ Department of physics, Dicle University, Diyarbakır, Turkey

\* Corresponding author; gulten@dicle.edu.tr

**Abstract:** *In this study, we investigated the structural, electronic and magnetic properties of the tetragonal LiRh₂Si₂ using the full-potential linearized augmented plane wave (FP-LAPW). The structural calculations were performed with four exchange and correlation potential (GGA- PBE, LDA-PW, GGA-WC and GGA-PBEsol), the electronic and magnetic properties were performed with GGA-PBE implemented in Wien2k code. We have obtained the cell dimensions, bulk modulus, and its pressure derivative.  The calculated lattice parameters are in good agreement with experimental and previous theoretical results. We calculated cohesive energy as 4,95 eV/atom and LiRh₂Si₂ has good stability. Electron density plot of LiRh₂Si₂ shows strong covalent interactions between Si-Si and Rh-Si elements. We performed spin polarize calculation of Density of States (DOS).  Electronic band chart that show LiRh₂Si₂ has metallic feature for both spin up and spin down configurations. The spin up and spin down electronic band chart nearly symmetric so the compounds has nonmagnetic feature. We searched pressure effect on magnetic moment of LiRh₂Si₂. The magnetic moment of  LiRh₂Si₂ has been found 0.00075 ( $\mu_B$ ) and it decreased with increase of pressure.*

Key words: *LiRh₂Si₂, Ab-initio calculations, Wien2k, FPLAPW, structural properties, magnetic properties, electronic properties*

## 1. Introduction

Lithium-transition metal-tetrelides (tetr. = C, Si, Ge, Sn, Pb) are an interesting class of compounds with respect to crystal chemistry and lithium mobility. Although many compounds with quite expensive noble metals have been studied, they are important model compounds in order to understand the structure–property relationships. These materials have intensively been investigated in recent years with respect to their structural chemistry and potential use as electrode materials in lithium batteries [1]. Nano- and bulk-silicon have intensively been studied in recent years with respect to lithiation for use as alternative electrode materials in lithium-ion batteries [2].

LiRh₂Si₂ and LiY₂Si₂ have been synthesized and investigated for structural and bond peculiar of them. Some theoretical works performed to investigate structural and bond chemistry of these materials [3].

Steinberg and Schuster (1979) synthesized and structural characterized of $LiY_2Si_2$ and $LiNd_2Si_2$ ternary compounds [4].

When we focus on this class of compounds we can see same studies on synthesis and some works focus on determine the physical properties. There are less theoretical study on these compounds and physical properties of $LiRh_2Si_2$ have not been studied in detail. That's why we focus on this study.

## 2. Computational method

The structural, electronic and magnetic properties of $LiRh_2Si_2$ were investigated by means of FP-LAPW method by using Wien2k package [5]. The cutoff energy, which defines the separation of valence and core states, was chosen as -7 Ry. The Muffin-tin sphere radii were selected 2,26 a.u. for Li 2,32 a.u for Rh and 1,7 a.u. for Si. The convergence of the basis set was controlled by a cut off parameter $R_{mt}*K_{max}$ was used 7, where $R_{mt}$ is the smallest of the MT sphere radii and $K_{max}$ is the largest reciprocal lattice vector used in the plane wave expansion. The magnitude of the largest vector in charge density Fourier expansion ($G_{max}$) was 12. We select the energy convergence as 0.0001 Ry and charge convergence as 0.001 e during self-consistency cycles. In these calculations, we neglected the effect of spin orbit coupling. For the Brillouin zone (BZ) integration, the tetrahedron method [6] with 195 special k points in the irreducible wedge (3000 k-points in the full BZ) was used to construct the charge density in each self-consistency step.

The structural calculation were performed with four exchange and correlation potentials (GGA-PBE, LDA, GGA-WC and GGA-PBEsol) [7-10] as implemented in Wien2k code.  We used  GGA-PBE potential for electronic and magnetic calculations.

$LiRh_2Si_2$ has tetragonal lattice with 127 (P4/mbm) space group (Fig.1). The atomic positions and cell dimensions of compounds are given in Table 1 [1].

Table 1. Unit cell parameters of $LiRh_2Si_2$

| Unit cell dimensions | a= 6,981 | c= 2,746 | |
|---|---|---|---|
| **Atomic coordinates** | **Li** | **Rh** | **Si** |
| | 0,  0,  0 | 0.14937,  $1/2 + x$,  1/2 | 0.3542, $1/2 + x$,  0 |

The calculations started with experimental data and searched for minimum energy depend of volume.  The electronic and optical calculations were performed with optimized structure parameters.
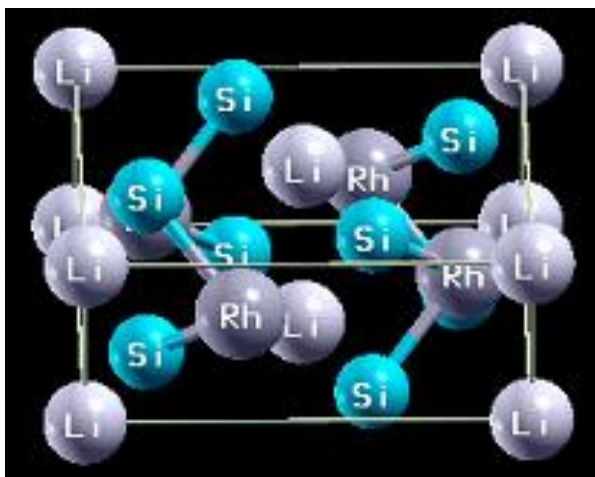
Figure 1. Unit cell of tetragonal LiRh₂Si₂ structure

## 3. Results and discussion

### 3.1. Structural properties

To find the ground state energy and optimize unit cell dimensions we calculate the total energy for diverse volume around experimental unit cell volume. The calculated total energies versus volume are fitted to the empirical Murnaghan's equation of state [11] to determine the ground state properties. The calculated total energy as a function of volume for four different potential and spin polarized PBE-GGA are plotted in Figure 2. We calculated ground state energy, unit cell volume, bulk modulus and derivative bulk modulus from structural optimization for each selected exchange correlation potentials. Calculated volume ($V_0$), bulk modulus ($B_0$), minimum energy (E) and derivative pressure ($B'$) values are given in Table 2.

Table 2. Calculated structural parameters of LiRh₂Si₂

| Values \ Potentials | $V_0$ ($au^3$) | $B_0$ (GPa) | $B'$ (GPa) | $E$ (Ry) |
|---|---|---|---|---|
| Nonmagnetic GGA-PBE | 925.1924 | 167.7183 | 4.4 | -40633.075959 |
| Spin polarize GGA-PBE | 924.2944 | 169.1183 | 4.4 | -40633.076791 |
| Nonmagnetic LDA | 879.7674 | 195.3441 | 4.5 | -40588.207521 |
| Nonmagnetic GGA-WC | 903.2018 | 180.9338 | 4.6 | -40626.066480 |
| Nonmagnetic GGA PBEsol | 898.1046 | 185.4190 | 4.6 | -40609.797268 |
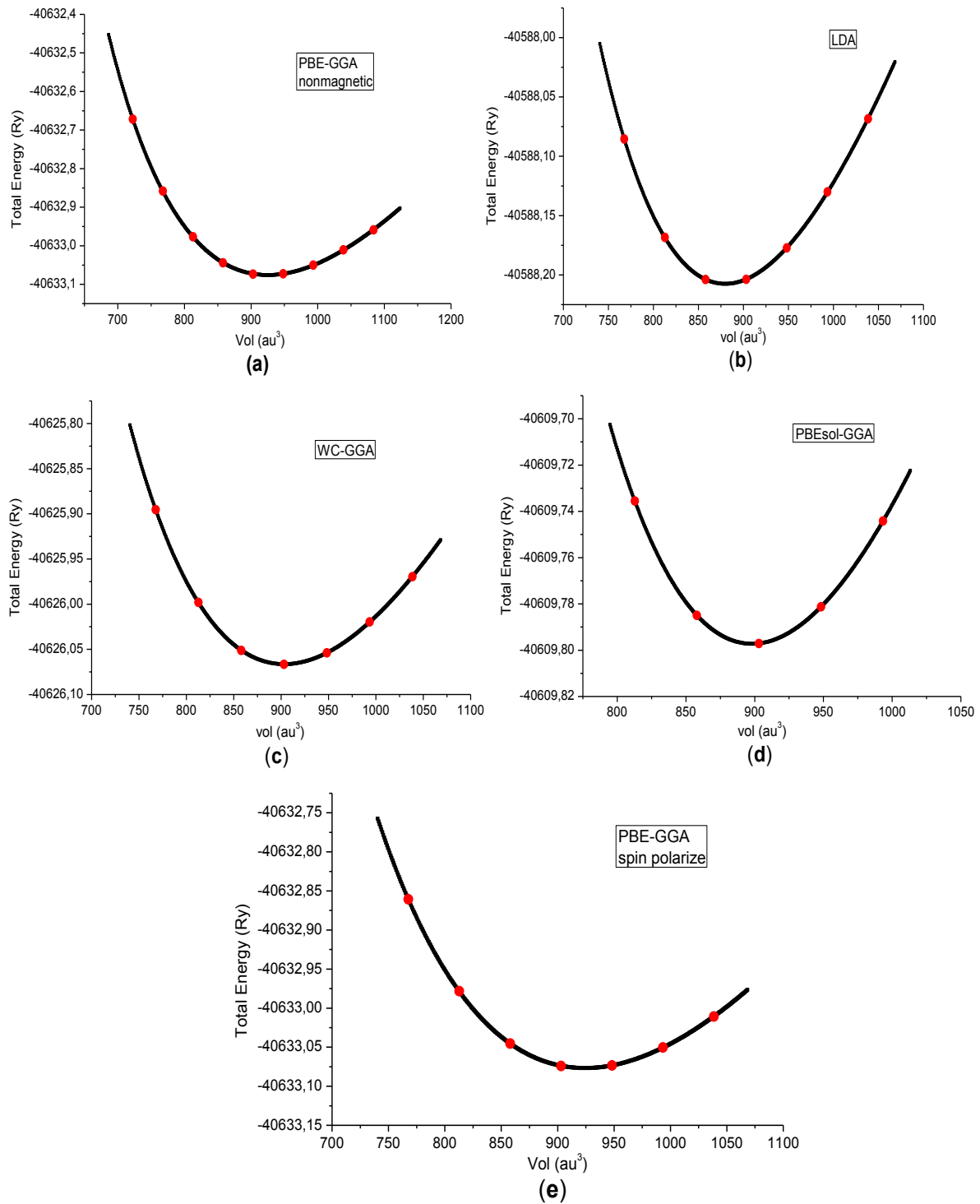
Figure 2. Dependence of total energy on unit cell volume of LiRh$_2$Si$_2$ with
a) Nonmagnetic PBE-GGA, b) LDA, c) WC-GGA, d) PBEsol,
e) Spin polarized PBE-GGA potentials

Experimental volume of LiRh$_2$Si$_2$ is 903,2 $au^3$ [1] and GGA-WC potential result is very close to it. Calculated bulk modulus has good agreement with previous calculated results, 200 GPa, in the LDA [1].

The structural stability of cell is confirmed by cohesive energy calculation. According to cohesive energy [12]

$$E_{coh} = -\frac{E_{LiRh_2Si_2}^{tot} - aE_{Li}^{tot} - bE_{Rh}^{tot} - cE_{Si}^{tot}}{a+b+c} \quad (1)$$

Where $E_{LiRh_2Si_2}^{tot}$, $E_{Li}^{tot}$, $E_{Rh}^{tot}$, $E_{Si}^{tot}$ are total energy of LiRh$_2$Si$_2$ unit cell, isolated Li, Rh and Si atoms, respectively. a, b and c indexes refer to the number of each atoms in the cell. We obtained the value of cohesive energy as 4,95 eV/atom for tetragonal LiRh$_2$Si$_2$.

### 3.2. Electronic and magnetic properties

It is well known that the electronic band structure and density of states (DOS) are important quantities to determine the crystal structure [12, 13]. In order to understand bonding character clearly, the total and partial densities of states (DOS) is calculated in Figure 3. Calculated DOS for spin up and spin down is given in Figure 4 are nearly symmetric and LiRh$_2$Si$_2$ has metallic feature for both spin. We plotted an electronic band chart   for spin up and spin down to understand the electronic properties of the structure (Fig.5). In this figure the Fermi energy level set to origin.  Spin up and spin down band charts are nearly same and has metallic feature.
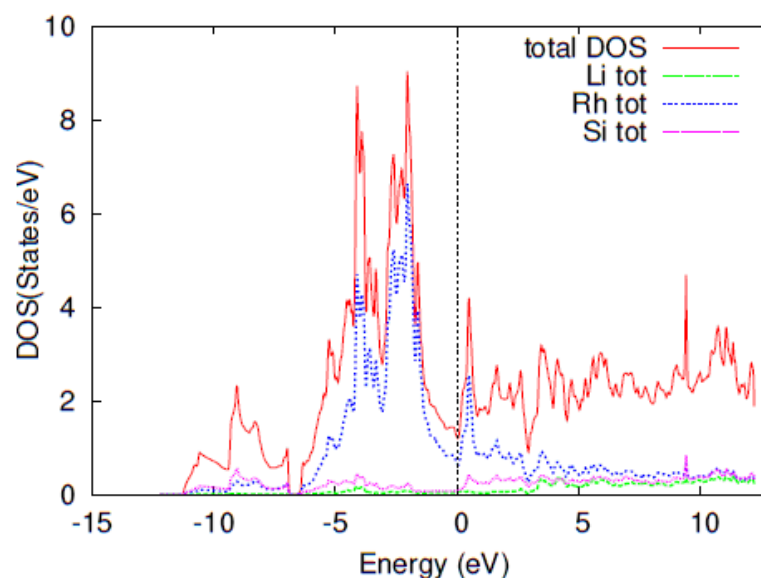


Figure 3. Calculated total and partial DOS of LiRh$_2$Si$_2$
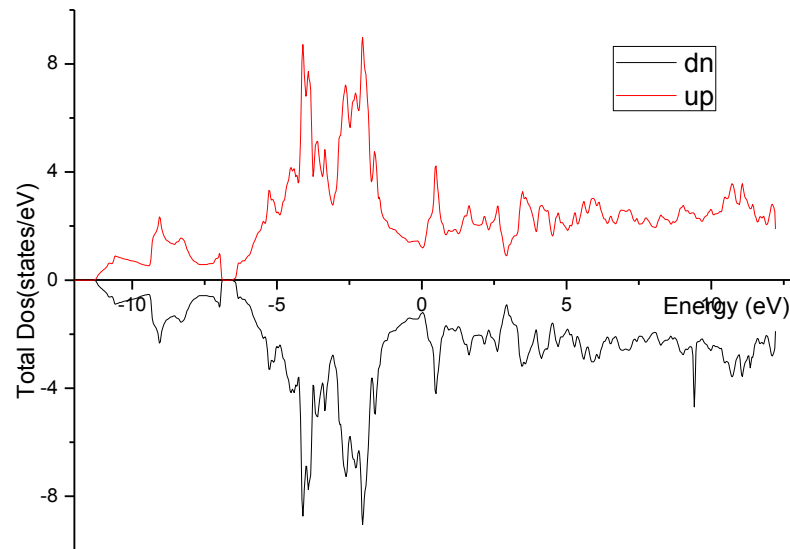
Figure 4. Density of states (DOS) of $LiRh_2Si_2$ with spin up and spin down configurations
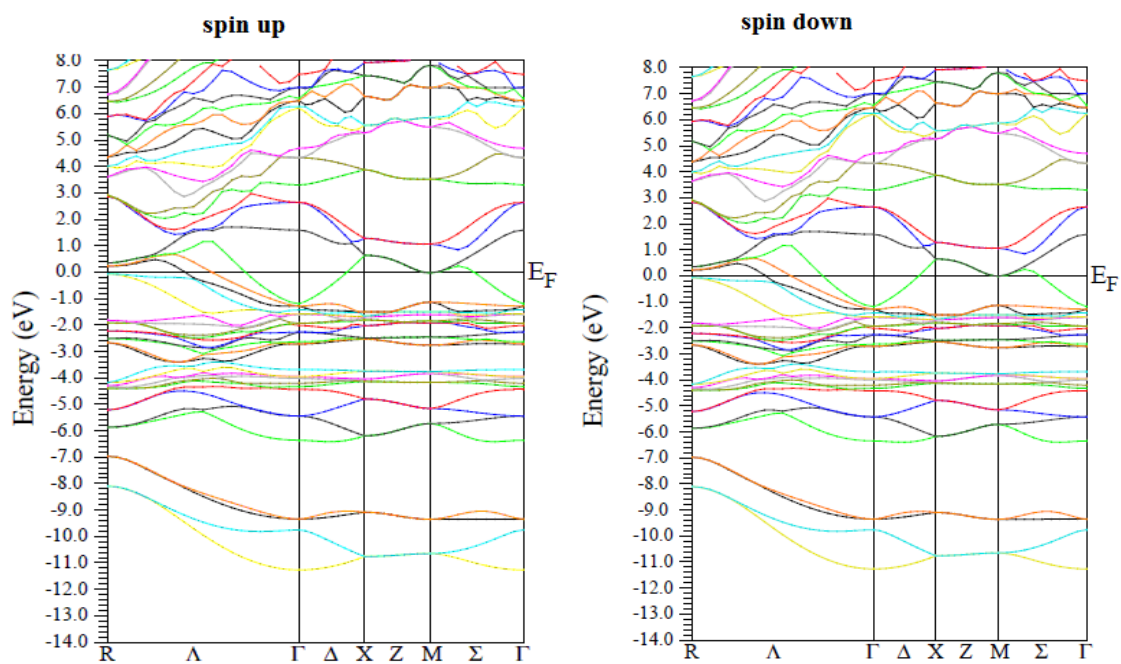


Figure 5. Band structure of $LiRh_2Si_2$ with (a) spin up and (b) spin down configurations.

We calculated electron density plots to understand bond characters of $LiRh_2Si_2$ in Figure 6. Charge distribution shows that there are strong covalent bond with Si-Si and Rh-Si elements.

(a)                                                                (b)
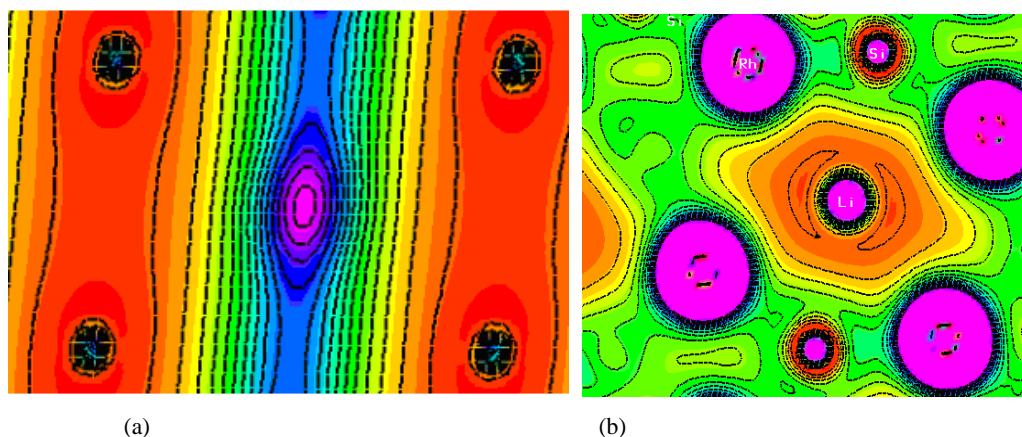
Figure 6.   Electron density plot of LiRh$_2$Si$_2$ with (a) 100 plate  ( b) 110 plate

To study the magnetic properties of the intermetallic LiRh$_2$Si$_2$ compounds, spin polarized calculations with the GGA (PBE) were performed. The total, interstitial and local magnetic moments of the compounds under investigation are summarized in Table 3.  The structure is paramagnetic with experimental cell dimensions and became diamagnetic with pressure.

Table 3. Calculated total, interstitial and local magnetic moments of the
compounds with GGA-PBE

| Pressure (Gpa) | $m^{int}$ | $m^{Li}$ | $m^{Rh}$ | $m^{Si}$ | $m^{cell}$ |
|---|---|---|---|---|---|
| 0 | 0.00042 | -0.00049 | 0.00027 | 0.00005 | 0.00075 |
| 14.89 | 0.00030 | -0.00019 | -0.00002 | -0.00002 | -0.00023 |
| 25.3 | -0.00188 | -0.00096 | -0.00052 | 0.00002 | -0.00578 |

**4. Conclusions**

We have searched structural, electronic and magnetic properties of tetragonal LiRh$_2$Si$_2$ structure using all electrons full potential linearized augmented plane wave (FPLAPW) method based on DFT within the  generalized gradient approximation (GGA) implemented in Wien2k code.  We calculated ground state energy unit cell dimensions and cohesive energy values.  The calculated cell constants are good agreement with experimental and previous theoretical works.   Calculated electron density plot and dos plot show that there are strong covalent bond with Si-Si and Si-Rh elements.  The calculated electronic band structure shows that LiRh$_2$Si$_2$ has metallic character both with spin up and spin down

configuration. $LiRh_2Si_2$ show paramagnetic feature with experimental unit cell constants and became show diamagnetic feature with increasing the pressure.

**References**

[1]  Pöttgen,  *et al.,*  "Lithium-transition metal- tetrelides structure and mithium Mobility", *Z. Phys. Chem.* 224, 1475–1504, 2010.

[2]  Langer,  *et al*.,  **"$^7$Li and $^{29}$Si Solid State NMR and Chemical Bonding of $La_2Li_2Si_3$",** *Solid State Sci.,* 14, 367-374, 2012.

[3]  Dinges,  *et al.,* " New ternary silicide $LiRh_2Si_2$ - structure and bonding peculiarities",  *Z. Anor. Chem.* 635, 1894-1903, 2009.

[4] Steinberg, G., Schuster, H., "Ternäre silicide des lithiums mit yttrium oder neodym mit modifizierter U3Si2-struktur", *Z. Naturforsch. B,* 34, 1237-1239, 1979.

[5] Blaha, *et al., An augmented  plane wave+ local orbitals program for calculating crystal properties*, Vienna, Austria, ISBN 3-9501031-1-2, 2001.

[6] Blochl, *et al.,* "Improved tetrahedron method for Brillouin-zone integrations", *Phys. Rev. B, 49*, 16223-16233, 1994.

[7]  Perdew, *et al.,* "Generalized gradient approximation made simple", *Phys. Rev. Lett.,* 77, 3865, 1996.

[8] Perdew, J.P., Wang, Y., "Accurate and simple analytic representation of the electron-gas correlation energy", *Phys. Rev. B,* 45, 13244-13249, 1992.

[9] Wu, Z.,  Cohen, R.E., " More accurate generalized gradient approximation for solids", *Phys. Rev. B,* 73, 235116, 2006.

[10]  Perdew, *et al.,* "Restoring the density-gradient expansion for exchange in solids and surfaces", *Phys. Rev. Lett.,* 100, 136406, 2008.

[11] Murnaghan, F.D., "The compressibility of media under extreme pressure", *Proceedings of the National Academy of Sciences of the United States of  America, Vol.30*, 1944, pp. 244-247.

[12] Naseri, *et al.,* "Electronic and optical properties of pentagonal-$B_2C$ monolayer: A first-principles calculation",  *Int. J. Mod. Phys. B,* 31, 1750044, 2017.

[13] Erdinc,  *et al.,*  "Ab-initio calculations of physical properties of alkali chloride XCl (X = K, Rb and Li) under pressure", *Computational Condensed Matter*, 4, 6-12, 2015.

# STABILITY ANALYSIS FOR THE KAWACHARA AND MODIFIED KAWACHARA EQUATIONS

*Mustafa MIZRAK*[*1]

[1]*Department of Computer Engineering, Faculty of Engineering, Şırnak University, Şırnak, Turkey* [*]

*Mustafa MIZRAK; mmizrak@sirnak.edu.tr*

**Abstract:**  *In this paper, by using the extended direct algebraic method, we obtain the exact traveling wave solutions for the Kawachara equation and the modified Kawachara equation. The exact solutions of the Kawachara and modified Kawachara equations demonstrated by graphs. The stability of these solutions and the movement role of the waves by sketching the graphs of the exact solutions are analyzed.*
Key words*: Traveling wave solutions, Extended direct algebraic method, Kawachara equation, modified Kawachara  equation*

## 1. Introduction

Many physical, chemical and biological phenomena such as combustion waves, optical solitons, chemical reactions, propagation of dominant genes and nerve pulses etc. are modelled by nonlinear partial differential equations exhibiting traveling wave solutions [1].

Traveling wave solutions of partial differential equations are solutions of special shape which do not change in time. The existence of such solutions for parabolic equations was first studied by A.N. Kolmogorov, I.G. Petrovskii, and N.S. Piskunov in their mathematical investigations of the equation proposed by R.A. Fisher in 1937 to describe the propagation of an advantageous gene.

Traveling wave solutions of partial differential equations are solutions of the form  *u(x;t) = f(x-ct),* with *x* being the spatial variable, *t* the time variable and *c* the constant speed of propagation of the wave. The properties of such solutions at different moments of time are obtained from one another by means of simple translation [2]. The investigation of exact traveling wave solutions to nonlinear evolution equations plays an important role in the study of nonlinear physical phenomena. Solitons are the most important solutions among traveling wave solutions [3].

The word soliton was discovered (and named) in 1965 by Zabusky and Kruskal, who experimenting with the numerical solution by computer of KdV equation. The word soliton was coined by Zabusky and Kruskal after "photon", "proton", etc., to emphasize that a soliton a localized entity which may keep its identity after an interaction [4].

In this study, we applied the extended direct algebraic method to find soliton solutions of Kawachara and Modified Kawachara equations.

## 2. Analysis of the extended direct algebraic method

The following is a given nonlinear partial differential equations with two variables $x$ and $t$ as where

$$P(u, u_x, u_t, u_{xx}, u_{xt}, u_{tt}, ...) = 0, \qquad (1)$$

$P$ is a polynomial function with respect to the indicated variables or some functions which can be reduced to a polynomial function by using some transformations.

**Step 1**: Assume that Eq. (1) has the following formal solution as:

$$u(x,t) = u(\xi) = \sum_{i=0}^{m} a_i \vartheta^i(\xi), \qquad (2)$$

where

$$\vartheta' = \sqrt{\alpha \vartheta^2 + \beta \vartheta^4} \qquad \text{and} \quad \xi = kx + \omega t, \qquad (3)$$

where $\alpha, \beta$ are arbitrary constants and $k$ and $\omega$ are the wave length and frequency and $\vartheta' = \dfrac{d\vartheta}{d\xi}$.

**Step 2**: Balancing the highest order derivative term and the highest order nonlinear term of Eq. (1), and the coefficients of series $\alpha, \beta, a_0, a_1, a_m, k, \omega$ are parameters can be determined.

**Step 3**: Substituting from Eqs. (2) and (3) into Eq. (1) and collecting coefficients of $\vartheta^i \vartheta^{(i)}$, then setting coefficients equal zero, we will obtain a set of algebraic equations. By solving the system, the parameters $\alpha, \beta, a_0, a_1, a_m, k, \omega$ can be determined.

**Step 4**: By substituting the parameters $\alpha, \beta, a_0, a_1, a_m, k, \omega$ and $\vartheta(\xi)$ obtained in step 3 into Eq. (2), the solutions of Eq. (1) can be derived.

## 3. Stability analysis

Hamiltonian system is a mathematical formalism to describe the evolution equations of a physical system. By using the form of a Hamiltonian system for which the momentum is given as

$$M = \frac{1}{2} \int_{-\infty}^{\infty} u^2 d\xi, \qquad (4)$$

where $M$ is the momentum, $u$ is the traveling wave solutions in Eq. (2). The sufficient condition for soliton stability is

$$\frac{\partial M}{\partial \omega} > 0, \qquad (5)$$

where $\omega$ is the frequency [5-19].

## 4. The applications of the method

### 4.1. The Kawachara equation

The Kawachara equation describing nonlinear wave processes in dispersive system [5] as

$$u_t + uu_x + u_{xxx} - u_{xxxxx} = 0. \qquad (6)$$

Consider the traveling wave solutions (2) and (3), then Eq. (6) becomes

$$\omega u' + kuu' + k^3 u''' - k^5 u^{(5)} = 0. \qquad (7)$$

Balancing the nonlinear $uu'$ and highest order derivative $u^{(5)}$ in Eq. (7) gives $m = 4$. Suppose the solution of Eq. (6) in the form

$$u(\xi) = a_0 + a_1\vartheta + a_2\vartheta^2 + a_3\vartheta^3 + a_4\vartheta^4. \qquad (8)$$

By substituting (8) into Eq. (7) yields a set of algebraic equations for $a_0, a_1, a_2, a_3, a_4, \alpha, \beta, k, \omega$. The system of equations are found as

$$
\begin{aligned}
k^3 \alpha a_1 - k^5 \alpha^2 a_1 + \omega a_1 + k a_0 a_1 &= 0, \\
k a_1^2 + 8k^3 \alpha a_2 - 32 k^5 \alpha^2 a_2 + 2\omega a_2 + 2 k a_0 a_2 &= 0, \\
6k^3 \beta a_1 - 60 k^5 \alpha \beta a_1 + 3 k a_1 a_2 + 27 k^3 \alpha a_3 - 243 k^5 \alpha^2 a_3 + 3\omega a_3 + 3 k a_0 a_3 &= 0, \\
24 k^3 \beta a_2 - 480 k^5 \alpha \beta a_2 + 2 k a_2^2 + 4 k a_1 a_3 + 64 k^3 \alpha a_4 - 1024 k^5 \alpha^2 a_4 + 4\omega a_4 + 4 k a_0 a_4 &= 0, \\
-120 k^5 \beta^2 a_1 + 60 k^3 \beta a_3 - 2040 k^5 \alpha \beta a_3 + 5 k a_2 a_3 + 5 k a_1 a_4 &= 0, \\
-720 k^5 \beta^2 a_2 + 3 k a_3^2 + 120 k^3 \beta a_4 - 6240 k^5 \alpha \beta a_4 + 6 k a_2 a_4 &= 0, \\
7 k a_3 a_4 - 2520 k^5 \beta^2 a_3 &= 0, \\
4 k a_4^2 - 6720 k^5 \beta^2 a_4 &= 0. \quad (9)
\end{aligned}
$$

The solution of the system of algebraic equations, can be found as

$$
a_0 = -\frac{36}{169} - \frac{\omega}{k}, \quad a_1 = 0, \quad a_2 = 0, \quad a_3 = 0, \quad a_4 = \frac{105\beta^2}{169\alpha^2}, \quad \alpha = \frac{1}{52 k^2},
$$

$$
a_0 = \frac{-4k^3 \alpha + 16 k^5 \alpha^2 - \omega}{k}, \quad a_1 = 0, \quad a_2 = \frac{280}{13}(-k^2 \beta + 52 k^4 \alpha \beta), \quad a_3 = 0, \quad a_4 = 1680 k^4 \beta^2. (10)
$$

Substituting from Eqs. (10) into (8), the following solutions of Eq. (6) can be obtained as

$$
u_1(x,t) = -\frac{36}{169} - \frac{\omega}{k} + \frac{105}{169} \sec h^4 \left( \frac{1}{2k\sqrt{13}} (kx + \omega t) \right), \tag{11}
$$

$$
u_2(x,t) = -\frac{36}{169} - \frac{\omega}{k} + \frac{26880\beta^2 \exp\left(2/k\sqrt{13}(kx+\omega t)\right)}{169\left(1 - 4\beta \exp\left(1/k\sqrt{13}(kx+\omega t)\right)\right)^4}, \tag{12}
$$

$$
u_3(x,t) = -\frac{36}{169} - \frac{\omega}{k} + \frac{26880\beta^2 \exp\left(2/k\sqrt{13}(kx+\omega t)\right)}{169\left(\exp\left(1/k\sqrt{13}(kx+\omega t)\right) - 4\beta\right)^4}, \tag{13}
$$

$$
u_4(x,t) = \frac{-4k^3\alpha + 16k^5\alpha^2 - \omega}{k} + \frac{280}{13}(\alpha k^2 - 52 k^4 \alpha^2) \sec h^2 \left(\sqrt{\alpha}(kx+\omega t)\right) +
$$
$$
1680\alpha^2 k^4 \sec h^4 \left(\sqrt{\alpha}(kx+\omega t)\right), \tag{14}
$$

$$
u_5(x,t) = \frac{-4k^3\alpha + 16k^5\alpha^2 - \omega}{k} + \frac{4480}{13}\alpha(-k^2\beta + 52 k^4 \alpha \beta) \frac{\exp\left(2\sqrt{\alpha}(kx+\omega t)\right)}{\left(1 - 4\beta \exp\left(2\sqrt{\alpha}(kx+\omega t)\right)\right)^2} +
$$
$$
430080 k^4 \alpha \beta^4 \frac{\exp\left(4\sqrt{\alpha}(kx+\omega t)\right)}{\left(1 - 4\beta \exp\left(2\sqrt{\alpha}(kx+\omega t)\right)\right)^4}, \tag{15}
$$

$$u_6(x,t) = \frac{-4k^3\alpha + 16k^5\alpha^2 - \omega}{k} + \frac{4480}{13}\alpha(-k^2\beta + 52k^4\alpha\beta)\frac{\exp\left(2\sqrt{\alpha}(kx+\omega t)\right)}{\left(\exp\left(2\sqrt{\alpha}(kx+\omega t)\right)-4\beta\right)^2} +$$

$$430080k^4\alpha^2\beta^2\frac{\exp\left(4\sqrt{\alpha}(kx+\omega t)\right)}{\left(\exp\left(2\sqrt{\alpha}(kx+\omega t)\right)-4\beta\right)^4}. \tag{16}$$
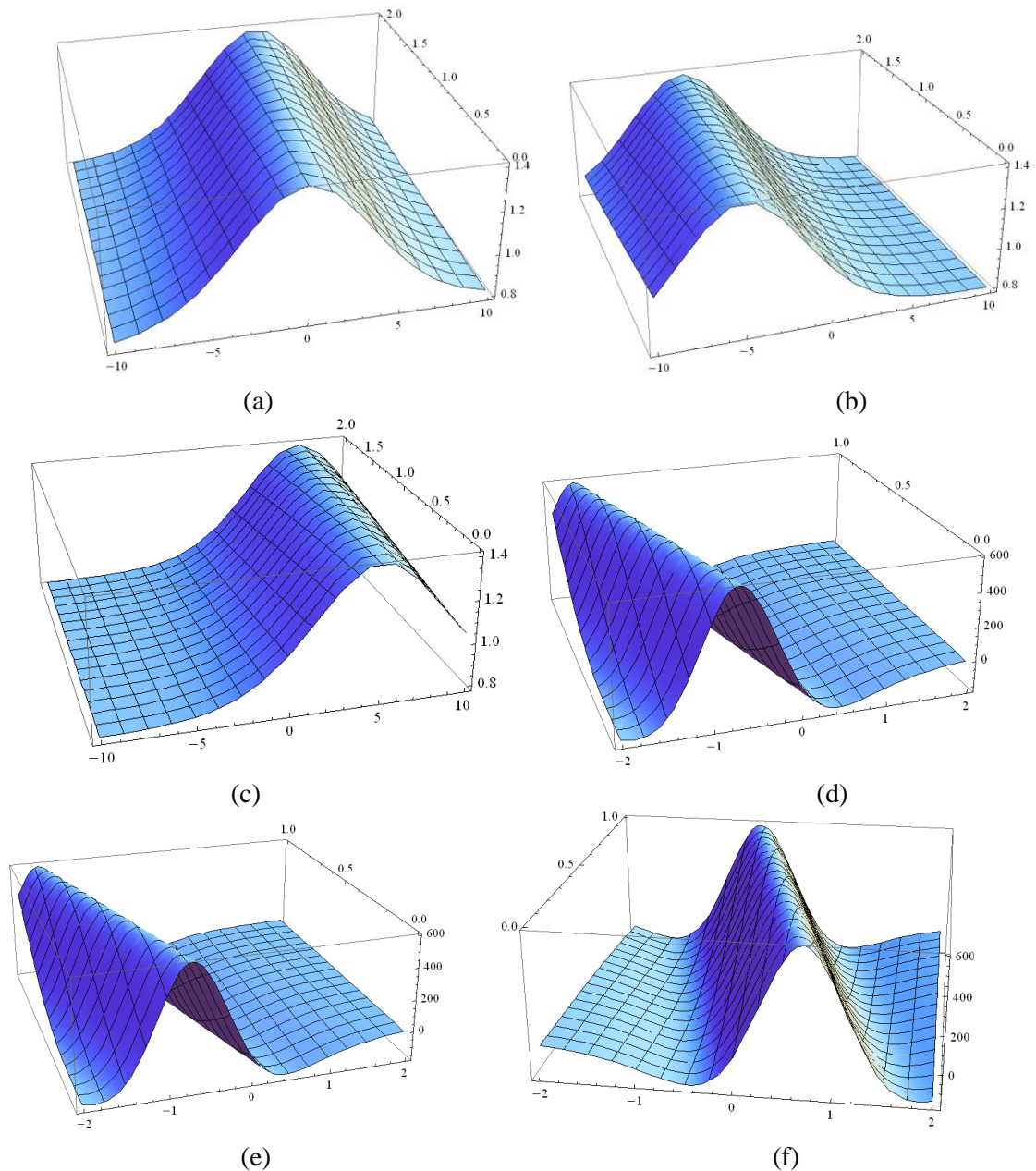


Fig 1. Traveling waves solutions (11)-(16) are plotted.

The traveling wave solutions (11)-(16) are shown in Fig. 1a-c   with   $\omega = \beta = -1$, $k = 1$  and $\alpha = 1/52$ in  the  interval  [-10,10]  and  [0, 2]; the  traveling  wave  solutions  (14)-(16)  are  shown  in

Fig.1d-f with $\omega = \alpha = k = 1$ and $\beta = -1$ in the interval [-2,2] and [0, 1]. According to the conditions of stability (4) and (5), the traveling wave solutions (11)-(13) are stable in the interval [-10,10] and [0, 2], the traveling wave solutions (14)-(16) are stable in the interval [-2,2] and [0, 1].

### 4.2. The Modified Kawachara equation

The modified Kawachara equation, which describes the motion of a water waves with surface tension as

$$u_t + u_x + u^2 u_x + p u_{xxx} + q u_{xxxxx} = 0, \qquad (17)$$

$p$ and $q$ are constants [10]. Consider the traveling wave solutions (2) and (3), then Eq. (17) becomes

$$u^2 u' + k^3 p u''' + q k^5 u^{(5)} = 0. \qquad (18)$$

Balancing the nonlinear $u^2 u'$ and highest order derivative $u^{(5)}$ in Eq. (18) gives $m = 2$. Suppose the solution of Eq. (18) in the form

$$u(\xi) = a_0 + a_1 \vartheta + a_2 \vartheta^2. \qquad (19)$$

By substituting (19) into Eq. (18) yields a set of algebraic equations for $a_0, a_1, a_2, \alpha, \beta, k, \omega, p, q$. The system of equations are found as

$$
\begin{aligned}
ka_1 + k^3 p \alpha a_1 + k^5 q \alpha^2 a_1 + \omega a_1 + k a_0^2 a_1 &= 0, \\
2k a_0 a_1^2 + 2k a_2 + 8k^3 p \alpha a_2 + 32 k^5 q \alpha^2 a_2 + 2\omega a_2 + 2k a_0^2 a_2 &= 0, \\
6k^3 p \beta a_1 + 60 k^5 q \alpha \beta a_1 + 6k a_0 a_1 a_2 + k a_1^3 &= 0, \\
24 k^3 p \beta a_2 + 480 k^5 q \alpha \beta a_2 + 4k a_1^2 a_2 + 4k a_0 a_2^2 &= 0, \\
120 k^5 q \beta^2 a_1 + 5k a_1 a_2^2 &= 0, \\
720 k^5 q \beta^2 a_2 + 2k a_2^3 &= 0.
\end{aligned}
\qquad (20)
$$

The solution of the system of algebraic equations can be found as

$$a_0 = \mp i p \frac{i}{\sqrt{10q}}, \quad a_1 = 0, \quad a_2 = \frac{6a_0}{\alpha}, \quad \alpha = -\frac{p}{10qk^2}, \quad \omega = -k - 4k^3 p \alpha - 16 k^5 q \alpha^2 - k a_0^2. \quad (21)$$

Substituting from Eqs. (19) into (18), the following solutions of Eq. (17) can be obtained as

$$u_1(x,t) = \frac{ip}{\sqrt{10q}} - \frac{6ip}{\beta \sqrt{10q}} \sec h^2 \left( \frac{i\sqrt{p}}{k\sqrt{10q}} (kx + \omega t) \right), \qquad (22)$$

$$u_2(x,t) = \frac{ip}{\sqrt{10q}} + \frac{96 i p}{\sqrt{10q}} \frac{\exp\left( \dfrac{2i\sqrt{p}}{k\sqrt{10q}} (kx + \omega t) \right)}{\left( 1 - 4\beta \exp\left( \dfrac{2i\sqrt{p}}{k\sqrt{10q}} (kx + \omega t) \right) \right)^2}, \qquad (23)$$

19

$$u_3(x,t) = \frac{ip}{\sqrt{10q}} + \frac{96ip}{\sqrt{10q}} \frac{\exp\left(\dfrac{2i\sqrt{p}}{k\sqrt{10q}}(kx+\omega t)\right)}{\left(\exp\left(\dfrac{2i\sqrt{p}}{k\sqrt{10q}}(kx+\omega t)\right)-4\beta\right)^2}, \qquad (24)$$

$$u_4(x,t) = -\frac{ip}{\sqrt{10q}} + \frac{6ip}{\beta\sqrt{10q}} \ \sec h^2\left(\frac{i\sqrt{p}}{k\sqrt{10q}}(kx+\omega t)\right), \qquad (25)$$

$$u_5(x,t) = -\frac{ip}{\sqrt{10q}} - \frac{96ip}{\sqrt{10q}} \frac{\exp\left(\dfrac{2i\sqrt{p}}{k\sqrt{10q}}(kx+\omega t)\right)}{\left(1-4\beta\exp\left(\dfrac{2i\sqrt{p}}{k\sqrt{10q}}(kx+\omega t)\right)\right)^2}, \qquad (26)$$
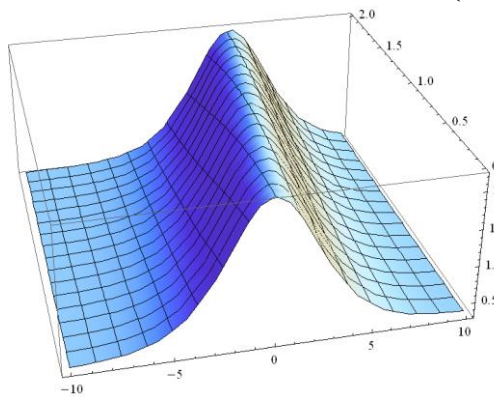
$$u_6(x,t) = -\frac{ip}{\sqrt{10q}} - \frac{96ip}{\sqrt{10q}} \frac{\exp\left(\dfrac{2i\sqrt{p}}{k\sqrt{10q}}(kx+\omega t)\right)}{\left(\exp\left(\dfrac{2i\sqrt{p}}{k\sqrt{10q}}(kx+\omega t)\right)-4\beta\right)^2}. \qquad (27)$$
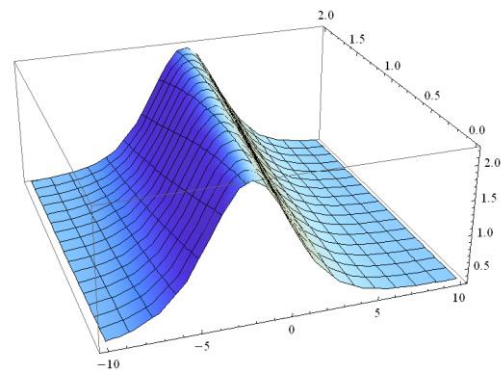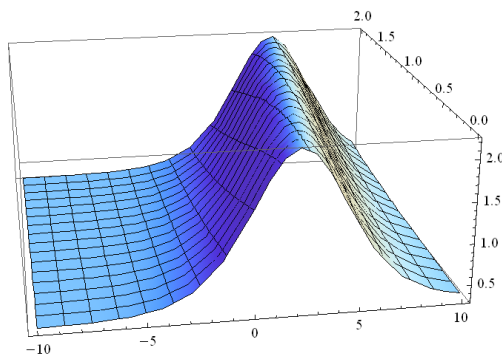


(a)



(b)



(c)



(d)

(e)                                                                              (f)
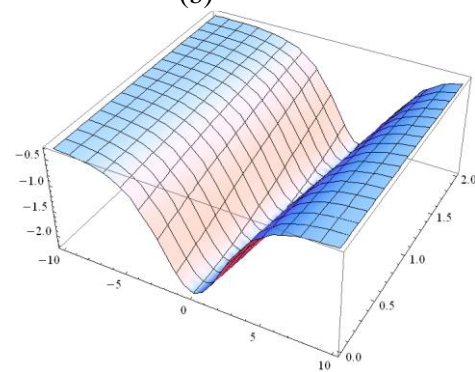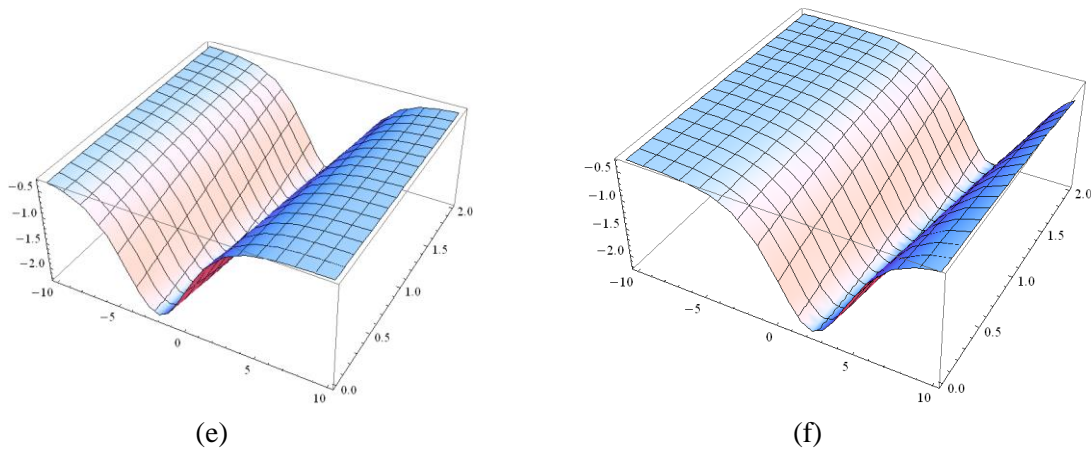
Fig 2. Traveling waves solutions (22)-(27) are plotted.

The traveling wave solutions (22)-(27) are shown in Fig. 2a-f with $p = k = 1,\ \beta = q = -1,\ \alpha = 0.1$ and $\omega = -1,34$ in the interval [-10,10] and [0, 2]. According to the conditions of stability (4) and (5), the traveling wave solutions (22)-(27) are stable in the interval [-10,10] and [0, 2].

## 5. Conclusion

We have applied the extended direct algebraic method by using symbolic software (Mathematica) to construct a series of traveling wave solutions. Implementing the proposed method, we have demonstrated the traveling wave solutions of Kawachara and modified Kawachara equations. Also triangular, periodic, rational, Weierstrass and Jacobi doubly periodic solutions that could be obtained with applied method have been ignored. Obtained all these solutions are distinct and stable.

## References

[1] Gubernov, V. *et al*. "Numerical methods for the travelling wave solutions in reaction-diffusion equations", *ANZIAM J.*, *44 (E)*, C271-C289, 2003.

[2] Ndeffo Mbah, M.L. "Travelling wave solutions for PDEs", *African Institute for Mathematical Sciences,* 7, 1-34, June, 2005.

[3] Fan, E., Hon Y.C. "A series of travelling wave solutions for two variant Boussinesq equations in shallow water waves", *Chaos, Solitons and Fractals, 15,* 559-566, 2003.

[4] Helal, M.A. "Soliton solutions of some nonlinear partial differential equations and its applications in fluids mechanics", *Chaos, Solitons and Fractals*, *13*, 1917-1929, 2002.

[5] Seadawy, A. R., Lu, D. "Bright and dark solitary wave soliton solutions for the generalized higher order nonlinear Schrödinger equation and its stability", *Results in Physics*, *7*, 43-48, 2017.

[6] Seadawy, A. R.  *et al*. "Travelling wave solutions of the generalized nonlinear fifth-order KdV water wave equations and its stability"*, J. of Taibah University for Science*, *11*, 623-633, 2017

[7] Seadawy, A. R., "Stability analysis for Zakharov-Kuznetsov equation of weakly nonlinear ion-acustic waves in a plasma", *Computers and Mathematics with Application, 67*, 172-180, 2014.

[8] Arshad, M. *et al., "* Travelling wave solutions of Drinfel'd-Sokolov-Wilson, Whitham-Broer-Kaup and (2+1)-dimensional Broer-Kaup-Kupershmit equations and their applications"*, Chinese Journal of Physic, 55*, 780-797, 2017.

[9] Kudryashov, N.A., "On types of nonlinear nonintegrable equations with exact solutions", *Physics Letters A*, *155*, 269-275, 1991.

[10] Ertas, A., Mızrak, M., Explicit Travelling Wave Solutions of Two Nonlinear Evolution
Equations, *Mathematical Sciences Letters*, *3(3)*, 223-228, 2014.

[11] Inc, M., Akgul, A., Kilicman, A., "Explicit Solution of Telegraph Equation Based on

Reproducing Kernel Method", *J. Func. Spaces and Apps,* Article Number: 984682, 2012.

[12] Inc, M., Akgul, A., Kilicman, A., "A New Application of the Reproducing Kernel Hilbert
Space Method to Solve MHD Jeffery-Hamel Flows Problem in Nonparallel Walls", *Abstract and
App. Analysis,* Article Number: 239454, 2013.

[13] Inc, M., Akgul, A., Kilicman, A., "Numerical Solutions of the Second-Order One-
Dimensional Telegraph Equation Based on Reproducing Kernel Hilbert Space Method", *Abstract
and App.  Analysis*, Article Number: 768963, 2013.

[14] Inc, M., Akgul, A., Kilicman, A., "Numerical Solution of Seventh-Order Boundary Value
Problems by a Novel Method", *Abstract and App. Analysis*, Article Number: 745287, 2014.

[15] Inc, M., Akgul, A., Kilicman, A. "Numerical solutions of fractional differential equations
of Lane-Emden type by an accurate technique", *Advances in Difference Eqs.,* Article Number:
220, 2015.

[16] Inc, M., Akgul, A., Kilicman, A., "On solitons and invariant solutions of the Magneto-
electro-Elastic circular rod", *Waves in Random and Coplex Media, V 26 Issue 3,* 259-271, 2016.

[17] Inc, M., Akgul, A., Kilicman, A., "Solitary Wave Solutions for the Sawada-Kotera
Equation", *J.  Adv.Physics,* 6(2)*,*288-293, 2017.

[18] Inc, M., Akgul, A., Kilicman, A., "Solutions of nonlinear systems by reproducing kernel
Method"*, J. Non. Sci. And Apps.,*10(8), 4408-4417, 2017

[19] Inc, M., Akgul, A., Kilicman, A., "On solutions of fractional Riccati differential equations",
*Advances in Difference Equations,* Article Number: 39. 2017.

# INVESTIGATION OF THE FORCE AND MOMENT EFFECTS OF ST 37 AND ST 70 ROOF LATTICE STEELS IN ANSYS PROGRAM

*Semih TAŞKAYA[1], Bilgin ZENGİN*[2], Kürşat KAYMAZ[3]*

[1]Department of Metallurgy and Materials Engineering, University of Firat, Elazig / TURKEY
*[2]Department of Electrical and Electronics Engineering, University of Munzur, Tunceli / TURKEY
[3]Department of Civil Engineering, University of Munzur, Tunceli / TURKEY

*Corresponding author; bilginzengin@munzur.edu.tr

**Abstract:** *St 37 and St 70 steels are the materials used in the manufacturing of general building materials, which are produced by processing the hot-formed steel further through a cold drawing process. Finite element method helps to simplify the complex engineering problems and to solve them with controllable parts. The roof lattice model simulated in the present study is a 4-surface pyramidal roof which is 4 mm in diameter, 0.5 mm in thickness and it was designed in 3D in Ansys software by using the finite element method. The bottom corner nodes of the roof lattice model were stabilized and the vector stress effects of 65.000 N force was applied in $F_x$, $F_z$ directions and 75.000 N force was applied in $F_y$ direction on the top node truss axes, 65.000 N.m moment was applied in $M_x$, $M_z$ directions and 75.000 N.m moment was applied in My direction on middle truss nodes were investigated. According to the test results in Ansys software, vector stress increase due to both force and moment effect in truss axes of the St 70 lattice roof steel compared to the St 37 steel.*

**Key words***: St 37- St 70, Ansys, Force and moment, Finite element method.*

## 1. Introduction

St 37 steel is a non-alloy steel.  Its mechanical properties are over 235 MPa of yield strength and 360-510 MPa of tensile strength. It is primarily used for riveting, screwing and welding purposes. St 37 structural steel material is utilized in many applications, combining its good welding properties with guaranteed strengths. There are various grades and uses including civil and industrial engineering. High strength low alloys have replaced many structural steels where weight reduction is important (e.g. automotive) but with guaranteed strengths [1]. Mechanical properties of St 70 steel are over 365 MPa yield strength and 690-900 MPa of tensile strength, and it is primarily used for riveting, screwing and welding purposes [2]. The finite element method is a promising tool in the modeling of several mechanical applications related to aerospace and civil engineering. One of the its  most exciting prospects is that it finds application on the coupled problems such as fluid-structure interaction, thermomechanical, thermochemical, thermo-chemo-mechanical problems, biomechanics, biomedical engineering, piezoelectric, ferroelectric, and electromagnetics [3]. In a study by Rottensteiner et al. (2014), the detection of roof planes from the analysis of three-dimensional (3D) point clouds and Digital Surface Models (DSMs) is an active research and application subject. Jochem et al. (2009) developed a representation of building spaces in 3-dimensional city models when roof planes were included in the models appropriately [5]. Huang et al (2013) used a generative modeling based on a primitive library for roof detection and reconstruction. The study also included combining the bottom-up and top-down approaches [6]. As suggested by Vitti (2012), areas with uniform gradient (i.e. planar) patches and boundaries (i.e. roof edges and eaves) can be detected by using the global variability model, which is a second-order model suggested by Blake and Zisserman (1987) [7-8]. Ohtake et al. (2004) performed an edge detection on triangular meshes by analyzing the principal curvatures and their derivatives [9]. Rottensteiner (2003) applied a region growing model on normal vectors in the production of the 3-dimensional building models [10]. Wang et al. (2013) considered the normal vectors as points on unit sphere, and then segmented planes and other orderly surfaces for detection [11].

## 2. Materials And Method

According to the finite element method in Ansys 12.0 software package, roof lattice modeling structure of St 37 and St 70 steels 3D design of a 4-surface pyramidal roof  with the dimensions of 4 mm in diameter and 0.5 mm in wall thickness was designed  according to the mechanical properties presented in Table 1 and Table 2.

**Table 1.** Mechanical properties of St 37 steel [12]

| Material | Density (kg/m³) | Elasticity Module (MPa) | Elongation (%) | Poisson Ratio | Tensile Strength (MPa) | Yield Strength (MPa) |
|---|---|---|---|---|---|---|
| **St 37** | 8000 | 210000 | 15 | 0.3 | 360-470 | 225-235 |

**Table 2.** Mechanical properties of St 70 [13]

| Material | Density (kg/m³) | Elasticity Module (MPa) | Elongation (%) | Poisson Ratio | Tensile Strength (MPa) | Yield Strength (MPa) |
|---|---|---|---|---|---|---|
| **St 70** | 7700 | 200000 | 8-25 | 0.3 | 650-880 | 350-550 |

### 2.1. Modeling

For the roof lattice model design by using the St 37 and St 70 steel standards, only one roof lattice profile was used for each element type. Following the various analyses on the same model, mechanical properties were identified and analysis was performed. In the first stage of the modeling, the analysis type is selected as "structural analysis". During the analysis of the model, the most significant parameter of element type is determined. Since the most commonly used process in roof lattice model is pipes, the element type is selected as "Pipe / elastic straight 16". The purpose of selecting this element type is to enable easy transfer of mechanical properties and achieve a solution. The mechanical data for the model are defined into the material characteristics module according to the Table 1 and Table 2. In the next stage, according to the coordinates given in Table 3, key points of 4 different roof surfaces are identified for each axis as shown in Figure 1 and a pyramidal roof model is generated.

**Table 3.** Key point measurements of the roof lattice model for each axis

| Measurements of Roof Lattice Surfaces | X | Y | Z |
|---|---|---|---|
|  | 0 | 0 | 0 |
|  | 35 | 0 | 0 |
|  | 60 | 0 | 0 |
| 1st Lattice Surface | 47.5 | 30 | 0 |
|  | 22.5 | 50 | 0 |
|  | 0 | 40 | 0 |
|  | 0 | 70 | 0 |
| 2nd Lattice Surface | -35 | 0 | 0 |

| | | | |
|---|---|---|---|
| | -60 | 0 | 0 |
| | -47.5 | 30 | 0 |
| | -22.5 | 50 | 0 |
| | 0 | 0 | 35 |
| | 0 | 0 | 60 |
| **3rd Lattice Surface** | 0 | 30 | 47.5 |
| | 0 | 50 | 22.5 |
| | 0 | 0 | -60 |
| | 0 | 0 | -35 |
| **4th Lattice Surface** | 0 | 30 | -47.5 |
| | 0 | 50 | -22.5 |

In Ansys 12.0 software package, coordinate data for lattice axes as given in Table 3 is entered into the system and a model similar to the one in Figure 1 is generated.
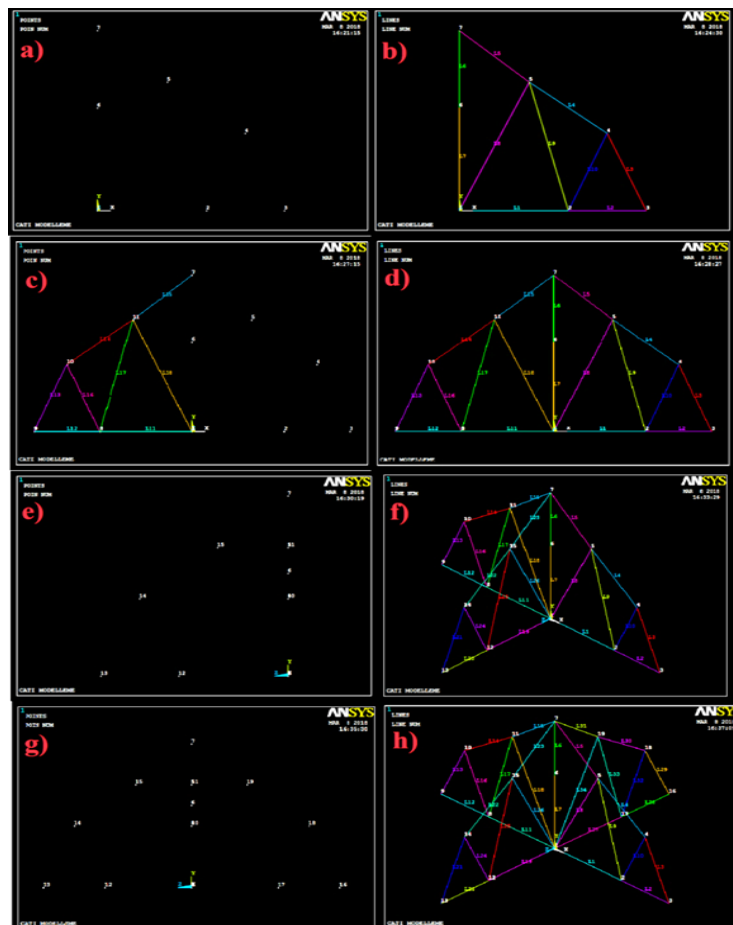
**Figure 1.** The roof lattice model shows the following: a) key points of the surface region in the 1st right front area - x direction  b) lines of the surface region in the 1st right front area - x direction c) key points of the surface region in the 2nd left front area - x direction d) lines of the surface region in the 2nd left front area - x direction e) key points of the surface region in the 3rd left  back area - z direction (view from the right in z direction) f) lines of the surface region in the 3rd left back area - z direction g) key points of the surface region in the 4th right back area -z direction (view from the right in z direction) h) lines of the surface region in the 4th right back area–z direction (completed roof lattice model)

After completing the coordinate measurements of the roof lattice model in all axes, the bottom base axes are assembled to the top node points as shown in Figure 2, thus the lattice points are strengthened.
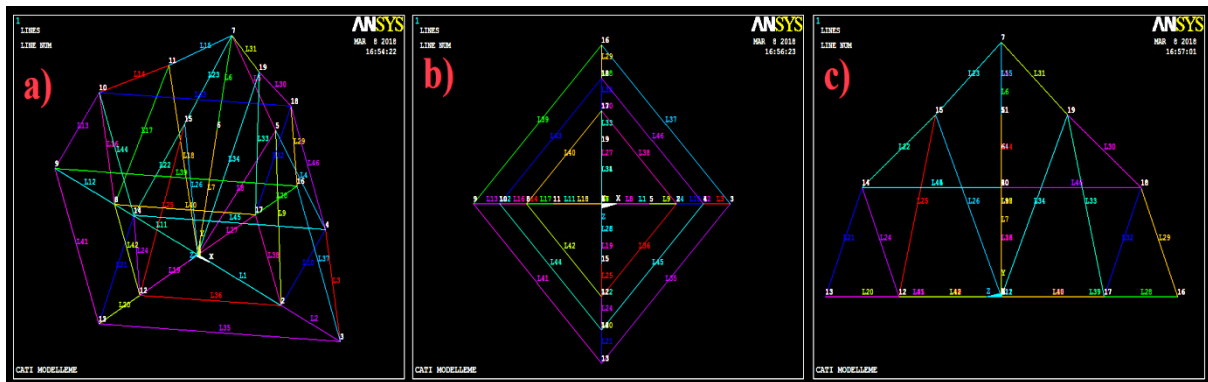


**Figure 2.** a) Assembly of the top node points to the bottom axes, b) view from below, c) right view of the truss axes from z axis direction of the roof lattice model

### 2.2. Mesh generation for the model

In the pyramidal-shaped roof lattice model, a meshing process was applied on steel pipes after the designing process for the distribution of mechanical properties. As the model is of a steel pipe, segmenting the meshing processes as 1-2 will be an ideal value for the solution. The value 1 was used for this mesh segmentation. After the meshing process as shown in Figure 3a, the pipe element size of these lattice pipes was selected "On" in the Ansys system as seen in 3b and the actual view of the roof lattice model in terms of diameter and thickness was generated.
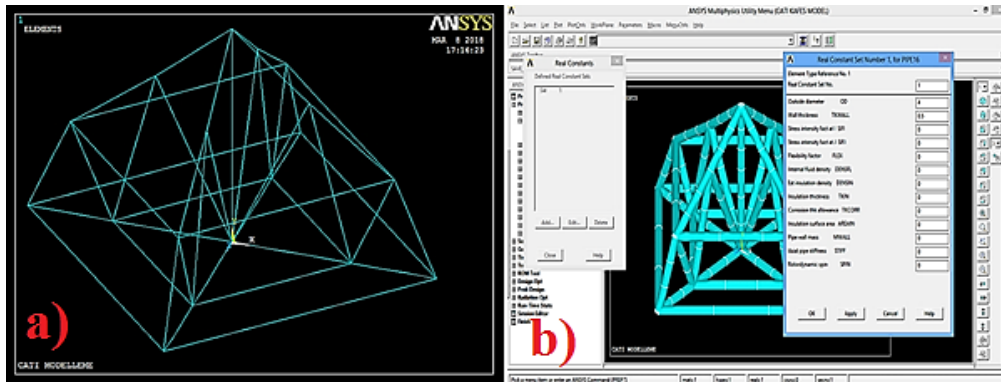
**Figure 3.** a) Mesh generation, b) entry of the pipe diameter and thickness values (4 mm pipe outer diameter, 0.5 pipe wall thickness) to the system for the roof lattice model

As Figure 2 shows the lines of model, Figure 4 shows the design views of the roof lattice model obtained from the residual element type from different perspectives.
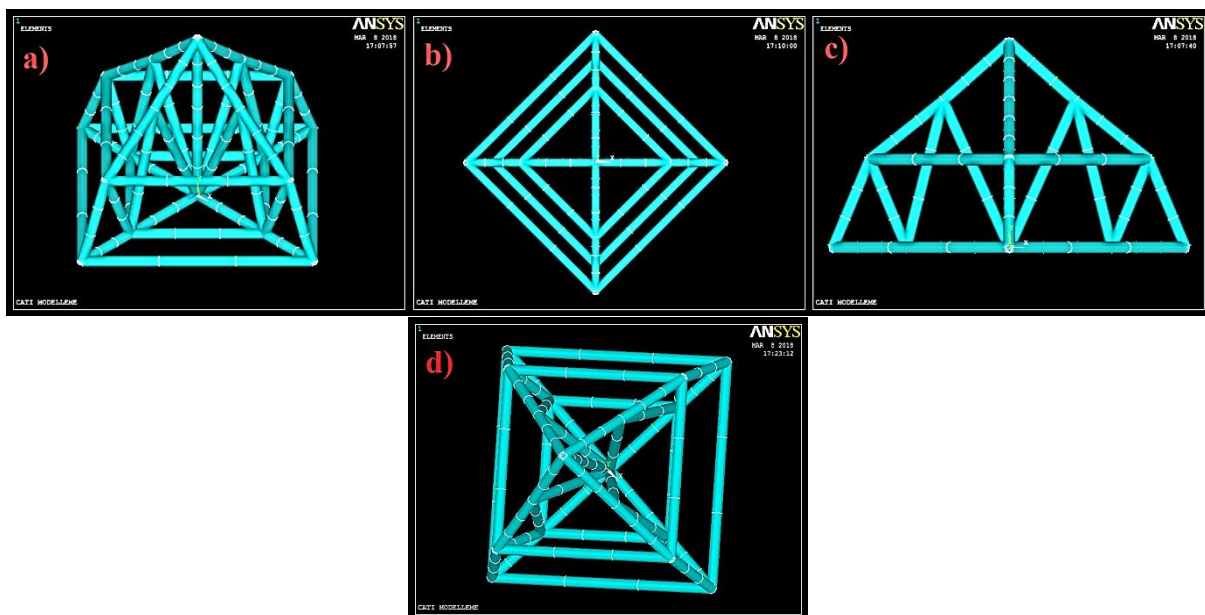


**Figure 4.** a) Front perspective element view, b) bottom perspective element view, c) perspective view from z direction to the truss axes, d) top perspective view of the roof lattice model

**2.3. Model stabilization; pressure and moment application process**

As it is shown in Figure 5a, the roof lattice model is stabilized from the bottom node points and analyzed to examine the mechanical effects of the steel type used in the model on force and moment (Figures 5c-6b). 65.000 N force in  $F_x$, $F_z$ directions and 75.000 N force in $F_y$ direction were applied on the top truss nodes, and 65.000 N.m moment in $M_x$, $M_z$ directions and 75.000 N.m moment (rotation effect) in $M_y$ direction was applied on the middle truss nodes of the pyramidal roof lattice (Figures 5b-6a). Deformation and vector quantities of all analyses induced by force and moment were investigated.
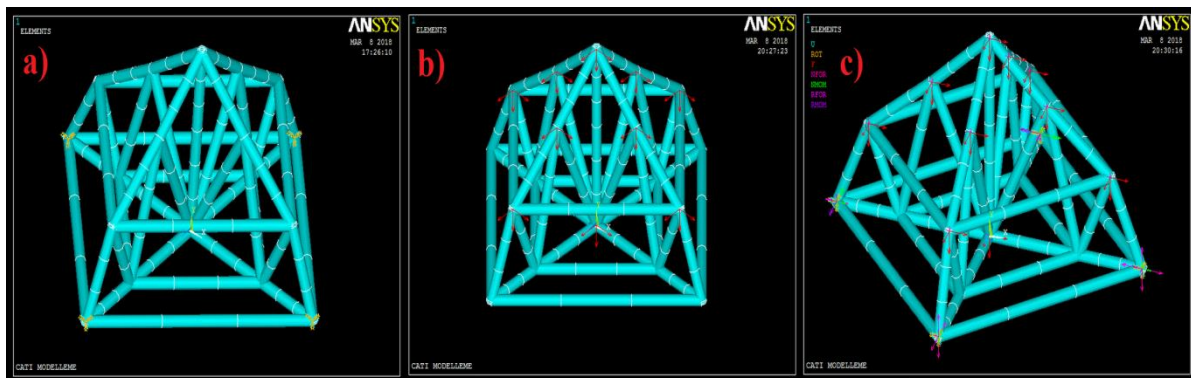
**Figure 5.** a) Stabilization of the roof lattice model from the bottom axes, b) moment application on truss nodes, c) display of the analysis result
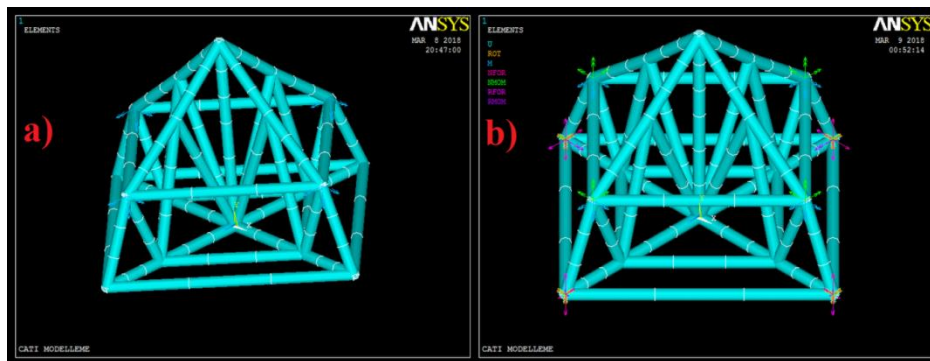


**Figure 6.** a) Moment application on middle truss nodes of the roof lattice model b) display of the analysis result

### 3. Results

#### 3.1. Force-induced mechanical analyses of the St 37 steel roof lattice

The model is analyzed after the effect of the force and moment applied on the St 37 and St 70 steel roof lattice pyramidal models. Following that, 138 elements and 111 nodes of the lattice are generated. Constructively, these elements and nodes yielded positive mechanical stress in the material. As shown in Figure 7, force-induced deformation (change in shape) and resultant vector change of the St 37 steel-type roof lattice are investigated.
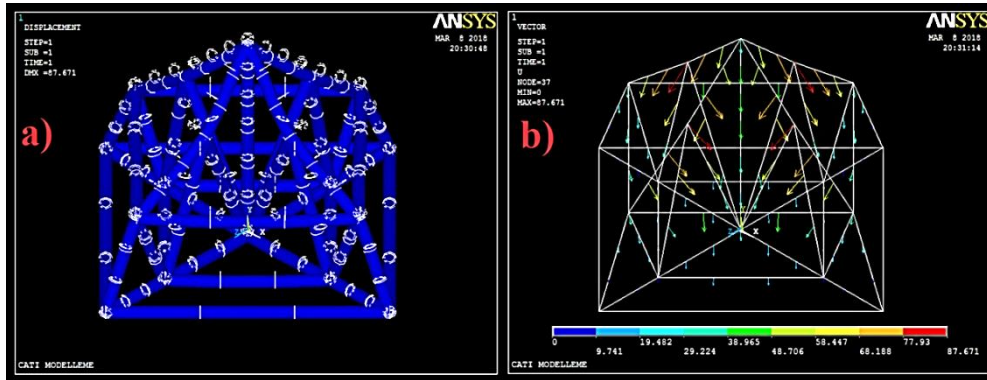
**Figure 7.** Force-induced a) deformation b) resultant vector quantitative analysis of the St 37 roof lattice model

As shown in Figure 8, axis-dependent mechanic vector changes of the St 37 steel-type roof lattice are investigated in terms of force.
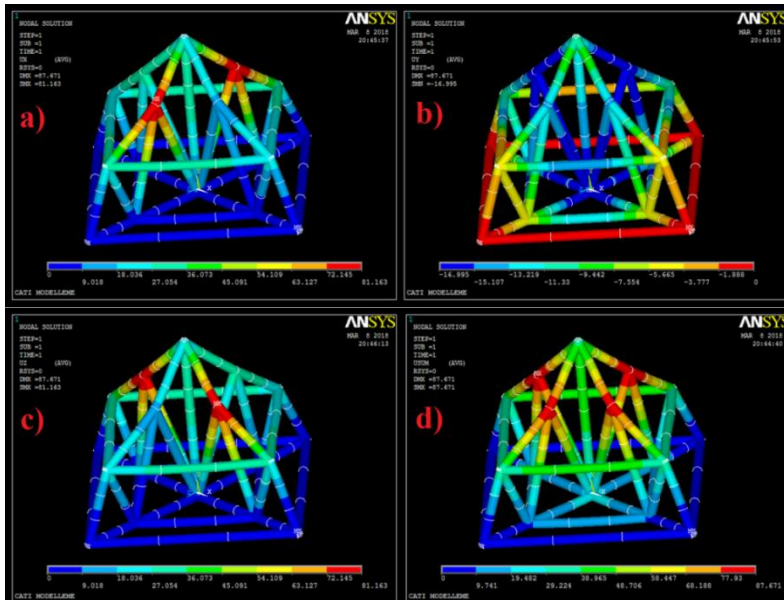


**Figure 8.** a) Vector node change in x axis, b) vector node change in y axis, c) vector node change in z axis, d) vector analysis in terms of the total distance between coordinate axes of the St 37 roof lattice model

### 3.2. Moment-induced mechanical analysis of the St 37 steel roof lattice

In Figure 9, moment-induced deformation (change in shape) and resultant vector change of the St 37 steel-type roof lattice are investigated.
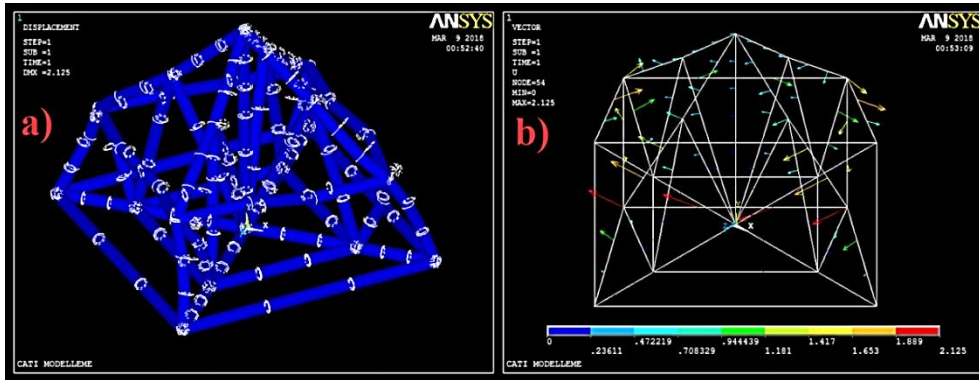
**Figure 9**. Moment-induced a) deformation b) resultant vector quantitative analysis of the St 37 roof lattice model

In Figures 10-11, moment vector change of St 37 steel-type roof lattice for each axis and node are investigated.
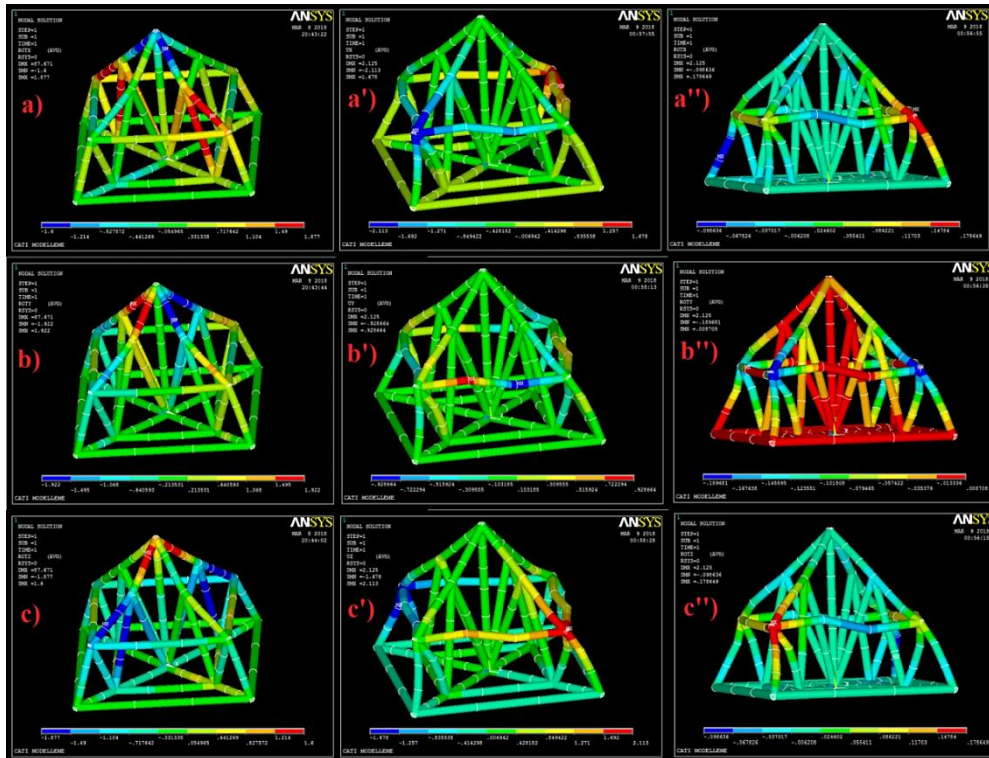


**Figure 10.** a) Rotation effect in x axis, a'') moment change effect of the nodes in x axis, a''') mechanic moment change effect in x axis, b) rotation effect in y axis, b'') moment change effect of the nodes in y axis, b''') mechanic moment change effect in y axis, c) rotation effect in z axis, c'') moment change effect of the nodes in z axis, c''') mechanic moment change effect in z axis of the St 37 roof lattice model in terms of moment.
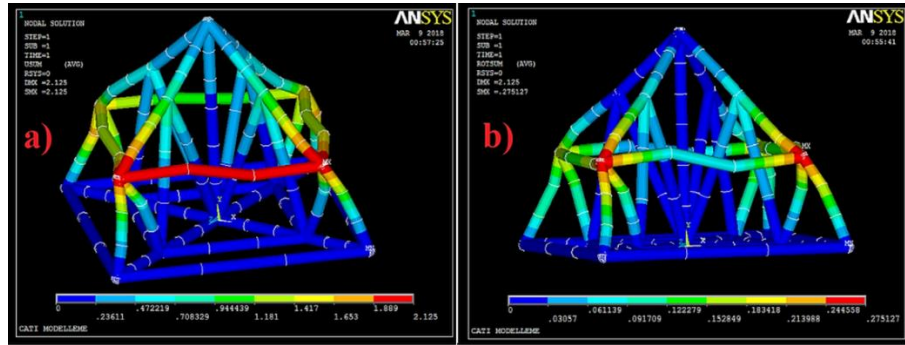
**Figure 11.** a) Total moment vector change in all coordinate points and b) moment change effect in all axis directions of the St 37 roof lattice model

### 3.3. Force-induced mechanical analyses of the St 70 steel roof lattice

Figure 12 shows the results of investigation of the St 70 steel type roof lattice in terms of the force induced deformation and resultant vector change.
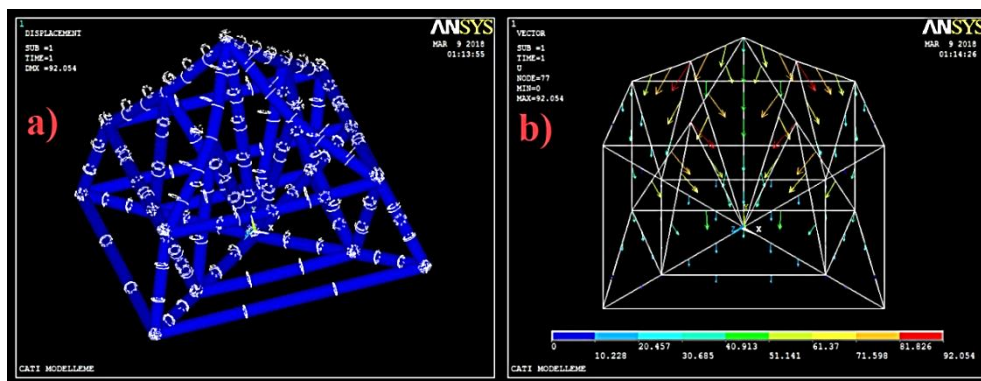


**Figure 12.** Force-induced a) deformation b) resultant vector quantitative analysis of the St 70 roof lattice model

Figure 13 shows the analysis of the mechanical changes of the roof cage of the St 70 steel type by the axes.
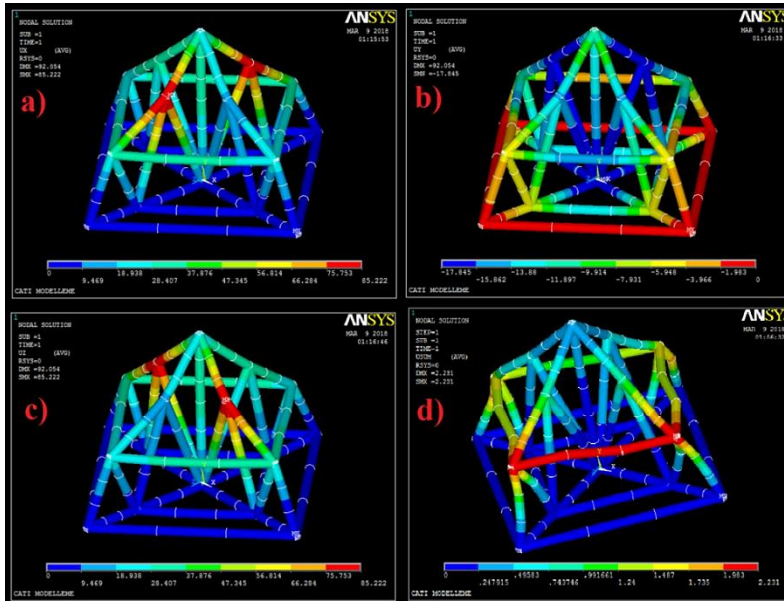
**Figure 13.** a) Vector node change in x axis, b) vector node change in y axis, c) vector node change in z axis, d) vector analysis in terms of the total distance between coordinate axes of the St 70 roof lattice model

### 3.4. Moment-induced mechanical analyses of St 70 steel roof lattice

Figure 14 shows the deformation and the vectorial change of the roof cage of St 70 steel type.
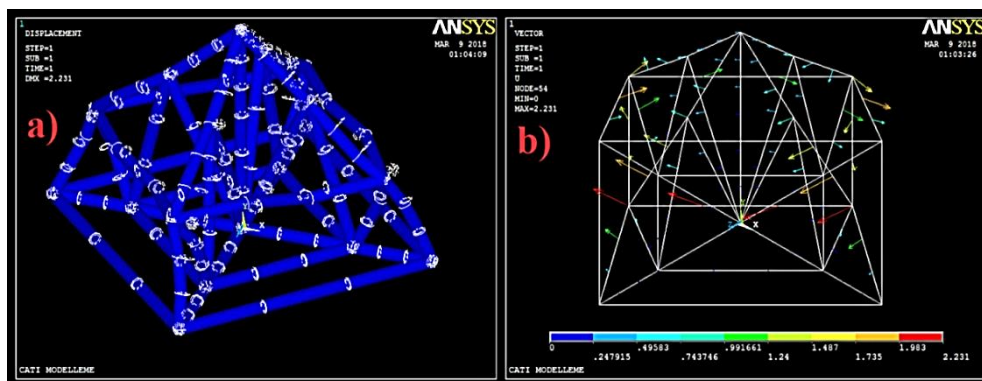


**Figure 14.** Moment-induced a) deformation (change in shape) and b) resultant vector quantitative analysis of the St 70 roof lattice model

In Figures 15-16, moment vector change analyses of St 70 steel type roof lattice for each axis and node are shown.
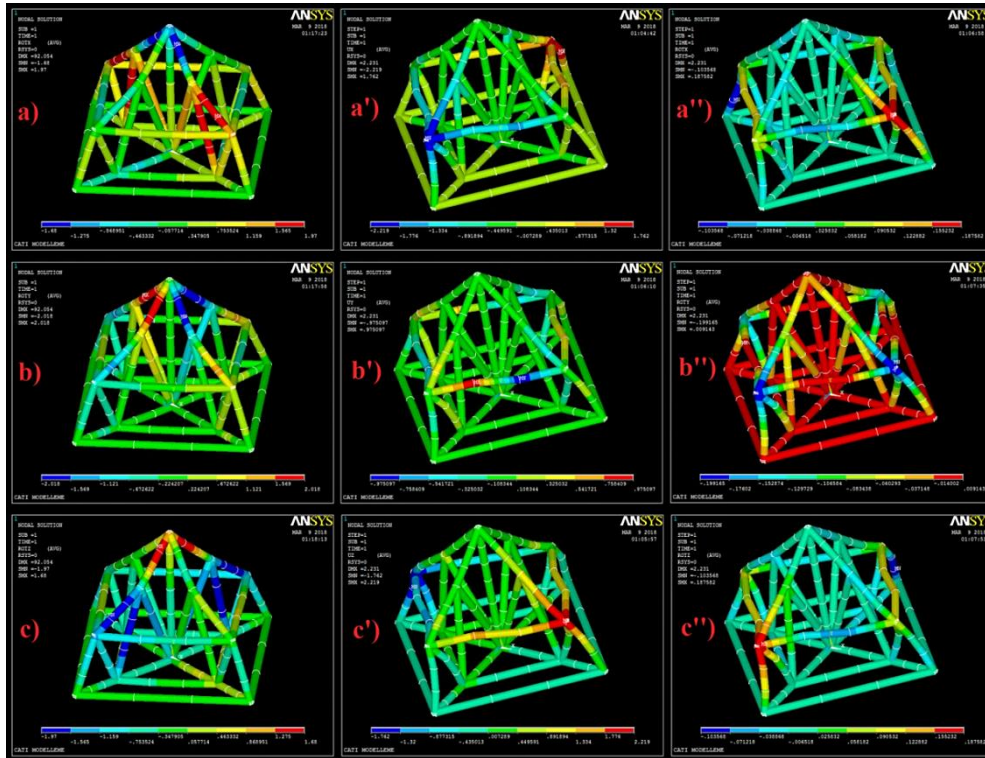
**Figure 15.** a) Rotation effect in x axis, a'') moment change effect of the nodes in x axis, a''') mechanic moment change effect in x axis, b) rotation effect in y axis, b'') moment change effect of the nodes in y axis, b''') mechanic moment change effect in y axis, c) rotation effect in z axis, c'') moment change effect of the nodes in z axis, c''') mechanic moment change effect in z axis of the St 70 roof lattice model in terms of moment.
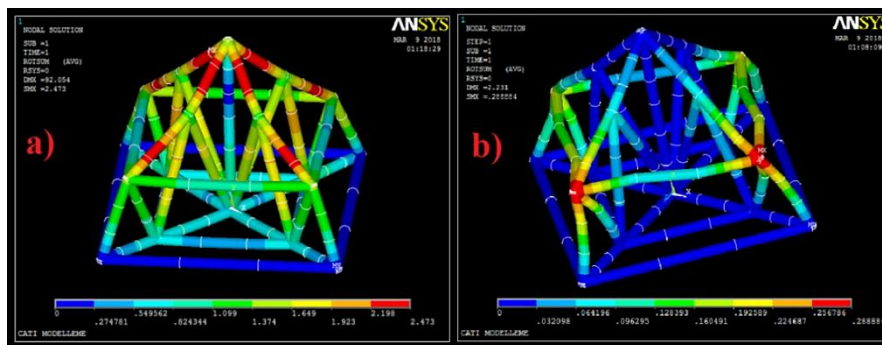


**Figure 16**. a) Total moment vector change in all coordinate points and b) moment change effect in all axis directions of the St 70 roof lattice model

In a comparison of mechanical analyses of St 37 and St 70 roof lattice steels in terms of force and moment, literature data shows that [12-13] the St 70 lattice steel has higher tensile strength, yield strength, lower density and elasticity module than the St 37 steel. Ansys simulation test analysis results demonstrate that program data validates these analysis results. That is, in force analyses of St 70 roof lattice steel compared to St 37 steel on truss node points, deformation as well as resultant

vector stresses and changes in coordinate points of all axes increase.  More vector node changings occur in steels with higher yield strength and tensile strength and lower elasticity module, because the trusses suffer from more constructive damage. Thus, mechanical stress is higher compared to the St 37 steel. On the other hand, the tensile strength of St 37 steel is low due to its higher elasticity module, therefore stretching is easier in trusses and less load is imposed on the truss nodes.

A comparison of moment changes caused by the rotation effect on roof lattice steels shows that it increased in St 70 steel in direct proportion to the result of force-induced mechanic vector simulation analyses. Similarly, due to the rotation effects in coordinate axes, the highest load accumulation in terms of tension and pressure movements was found in the St 70 roof lattice steel. Moment vector changes, rotation effects between axis nodes, resultant vector changes and deformation as well as the highest mechanical effect were observed in St 70 steel lattice trusses as compared to St 37 roof lattice steel.

## References

[1]    ***, Bebon International co., ltd., http://www.steel-plate-sheet.com/Steel-plate/DIN/St372.html

[2]     ***, Join-Win Steel, http://www.steel-jw.com/DINEN/ST702-structure-steel-with-competitive-price.html

[3]     ***, Simscale Blog-Finite Element Method, https://www.simscale.com/blog/2016/10/what-is-finite-element-method/

[4]     Rottensteiner, F., Sohn, G., Gerke, M., Wegner, J.D., Breitkopf, U., Jung, J., "Results of the ISPRS benchmark on urban object detection and 3d building reconstruction", *ISPRS J. Photogram. Remote Sens.,* 93, pp. 256-271, 2014.

[5]   Jochem, A., Höfle, B., Rutzinger, M., Pfeifer, N., "Automatic roof plane detection and analysis in airborne LiDAR point clouds for solar potential assessment", *Sensors*, 9, pp. 5241-5262, 2009.

[6]   Huang, H., Brenner, C., Sester, M., "A generative statistical approach to automatic 3D building roof reconstruction from laser scanning data", *ISPRS J. Photogram. Remote Sens.,* 79, pp. 29-43, 2013.

[7]    Vitti, A., "The Mumford-Shah variational model for image segmentation: an overview of the theory, implementation and use", *ISPRS J. Photogram. Remote Sens.,* 69, pp. 50-64, 2012.

[8]   Blake, A., Zisserman, A., *Visual Reconstruction,* MIT Press Cambridge, MA, USA, 1987.

[9]    Ohtake, Y., Belyaev, A., Seidel, H.P., "Ridge-valley lines on meshes via implicit surface fitting", *ACM Trans. Graph.,* 23, pp. 609-612, 2004.

[10]    Rottensteiner, F., "Automatic generation of high-quality building models from LiDAR data", *IEEE Comput. Graphics Appl.,* 23, pp. 42-50, 2003.

[11]   Wang, Y., Hao, W., Ning, X., Zhao, M., Zhang J., Shi, Z., Zhang, X., "Automatic segmentation of urban point clouds based on the gaussian map", *Photogram. Rec.,* 28, pp. 342-361, 2013.

[12]    Taşkaya S., "Investıgatıon of mechanical stresses dependent on press in St 37 steel Ansys program", *The Journal of International Manufacturing and Production Technologies (JIMPOT)*, 1, pp. 39-46, 2017.

[13]   ***, China steel suppliers, http://www.steelgr.com/Steel-Grades/Carbon-Steel/st70-2.html

# AN EXAMPLE TO THE CHANGE OF EARTH SHAPE: EVIDENCE OF TETHYS SEA IN DİYARBAKIR

*İhsan EKİN[1] \*, Rıdvan ŞEŞEN[2]*

[1]Department of Energy Systems Engineering, Faculty of Engineering, Şırnak University, Şırnak, Turkey
[2]Department of Biology, Faculty of Science, Dicle University, Diyarbakır, Turkey

*Correspondence: e-mail: ekinihsan@gmail.com

**Abstract:** *The change of earth shape over time is expressed as Geological Evolution. The German meteorologist Alfred Wegener (1880-1930) describes the geological evolution of the Continental Drift Theory, which means that terrestrial parts of the earth and large water bodies change over time. According to the Continental Drift Theory, during the Mesozoic Era, the large earth continent Pangaea was divided into two gigantic continents (Laurasia and Gondwana), forming the Tethys Sea. The Tethys Sea was connected to the present Indian Ocean through the Atlantic Ocean and the Mediterranean Sea. A large part of Anatolia, especially in Southeastern Anatolia, was covered with the sea for a long time. Today's both the Mediterranean and the Black Sea is considered as a remnant of Tethys Sea. These seas were also subjected to some other important changes. In the studies carried out within the province of Diyarbakır, the biological evidence of the Tethys Sea was found in invertebrate fossils. The marine form of fossils belonging to Echinodermata and Bivalvia phyla are frequently encountered in the Southeastern Anatolia Region. They were collected from the Diyarbakır province and photographed. The fossil specimens are of great importance in terms of understanding the geological changes (Geological evolution) that the region has undergone over time.*

Keywords*: Diyarbakır, Tethys Sea, Invertebrate fossils,*

## 1. Introduction

The concept of evolution essentially includes three sub-concepts: Inorganic Evolution, Organic Evolution, and Social Evolution [1]. Inorganic evolution studies the change of inanimate objects. In particular, it covers events from the formation of the universe to the formation of inanimate objects, which form the basis of living things. Some authors also use chemical and physical concepts of evolution for these changes over time. Geological Evolution is generally used for changes that take place in the forms of the earth [2, 3]. In this work, we adopted this statement and used the expression "Geologic Evolution" as many scientists have used. The content of our work includes the geological change that our region has undergone with the presence of the fossil record.

Organic evolution, however, examines the evolution of living things over time. The biological evolution that has begun from the moment when the first living things emerged (approximately 3.5 billion years ago) and still continues is the subject of the science of Biology in general. When it comes to evolution, it is generally desired to describe the Biological evolution and it is the most interesting concept of evolution. Social evolution examines the changes of societies over time. The change of societies over time is more a matter of sociology science. Changes are mostly on a cultural basis. In our work, it was thought that the use of "Geological Evolution" statement from the above-mentioned concepts of evolution is correct.

One of the most important theories about the transformation of the earth is the "Continental Drift Theory". This theory was first suggested by the German meteorologist Alfred Wegener in 1912, and the subsequent contributions bring in important benefits to the theory (Paleontological, geological and biological findings, and photographs taken from the space, seismic studies, and deep sea studies). According to this theory; at the beginning of the Mesozoic Era, all the earth continents were together in one piece. The Pangaea, large single continent, has been shattered throughout the Mesozoic Era and transformed into today's continents. Pangaea was first divided into the North and South continents. The north part is Laurasia; the southern part is called Gondwana. The sea of Tethys formed in the space between Laurasia and Gondwana. The name of Tethys Sea was first used by the Austrian geologist Edward Suess in 1893. Suess used this name based on the fossils of living creatures that existed only in the seas, both in the Alpine mountains and in parts of Africa at that time. This sea was thought more as an inner sea. Wegener used the term Tethys, however, explained the existence of the sea in a different way, according to the Continental Drift Theory. The sea of Tethys, as mentioned above, was linked to the Indian Ocean, covering a large part of today's North Africa and a large part of southern Europe and the Middle East on the Mediterranean Sea. In other words, it was a sea separating the two great continents, Gondwana and Laurasia. The sea of Tethys, formed by millions of years of change, has shrunk in time and has become almost an inland sea with its remains, like the Mediterranean. Once upon a time, when Anatolia was covered with the sea, due to the proximity of the African continent to the Asian and European continents, some island-shaped ascents have developed. Turkey, a young stratum, formed between Eurasia in the north and Africa-Arabia plates in the south [4]. This zone is occasionally covered with seas, depending on weather conditions and some other conditions. Southeastern Anatolia is finally assumed to be covered by the sea about 7 million years ago [5]. During the Era when Anatolia was covered with sea, some marine living creatures were preserved as fossils till today.
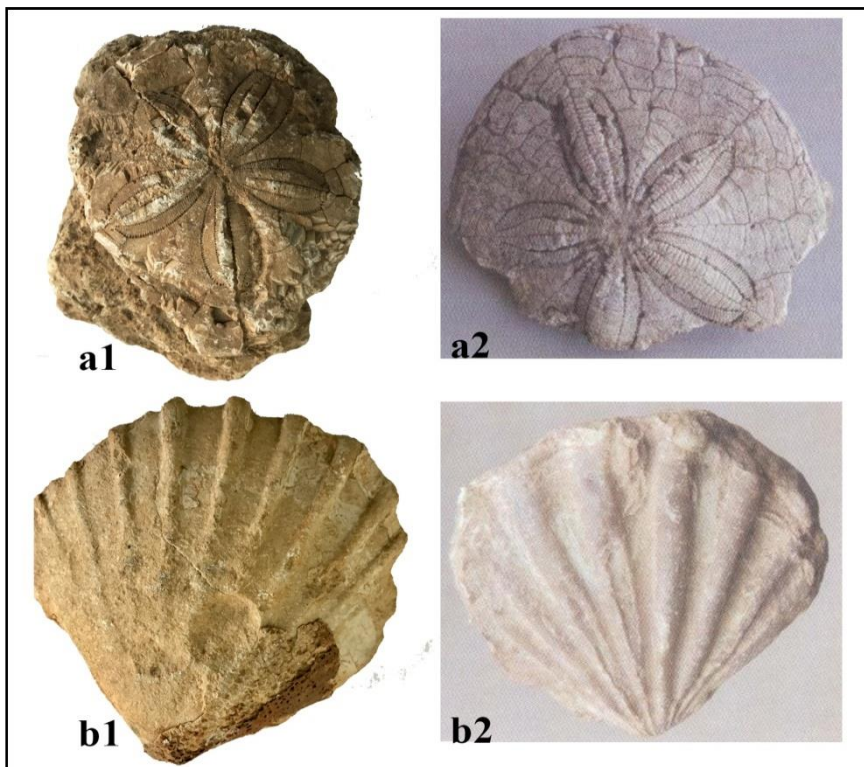
**Photograph 1. a1.** *Clypeaster* genus and **b1.** *Flabellipecten* genus, two fossils collected from the region between the Hani and Lice in Diyarbakir city. The photograph of these genera, which have already been recorded, is shown **a2.** *Clypeaster tauricus* and **b2.** *Flabellipecten cf. fraterculus* [4].

With the comparison of the photographs, the genera of the fossils are more or less understood. But it is not very accurate to say exact name of the species, a detailed investigation is required.

## 2. Material and Method

In order to be used in previous investigations, the fossil specimens were collected between 1990 and 2016 in Southeastern Anatolia region and brought to the laboratory of Biology Department. Fossils are found in the mountainous region between Lice and Hani district in Diyarbakır. The first fossils were identified at the phylum level. It is understood that the detected fossils generally belong to two important invertebrate phyla whose internal organs are covered with hard crust or interlocked plaques. The fossils were examined; their photographs were taken and maintained in the biology department for further studies.

## 3. Results

The collected fossils were first identified according to their Phyla. Most of the fossils belong to the Echinodermata Phylum (Photograph a1) and some of them belong to Bivalvia class, *Clypeaster* genus (Photograph b1).

Echinodermata is one of the most important invertebrate phyla that enter the group of Deuterostomia, which is also consisting of vertebrates. For this reason, this phylum is described in many books after the arthropods. The most important feature of this phylum is that all species have been living in the seas from the beginning to the nowadays. And generally, show radial symmetry of 5 in mature form. This phylum, which is regarded as real marine animals, is examined in 5 classes; Sea lilies (Crinozoa), Sea stars (Asteroidea), Brittle stars (Ophiuroidea), Sea urchins (Echinoidea) and Sea Cucumbers (Holothuroidea) [6]. A significant quantity of the fossils collected from the Diyarbakır belongs to the class of Sea urchins (Echinoidea) of Echinodermata phylum. The five radial symmetry structure in the fossils is obviously seen. Another important feature of this phylum is their tube feet which are used for various purposes by the animal. The holes of tube feet (interambulacral regions) that come out from the plates of the feet (ambulacral regions) are visible in the fossils (Photograph 2a). The holes in the tube legs can be counted on the fossil specimen (Photograph 2b). Fossilization is not easy as is known. It requires very special conditions. The most important environments in fossil formations are clayey and muddy environments, especially composed of fine particles. The living thing that has fallen or drifted into this mud anyhow, the elements around it become hardened and become fossilized in a real form. Then, the shell or crust can often disappear with decay, but the shape of the organism remains constant. If the minerals then fill in this mold, a new mold is formed again and a moulage of the organism occurs and gives a general outline of the living thing. If the body mold is filled with the only mineral, it is called calcification [7]. Our examples are petrified fossils thought to be formed as described above.

Another part of the fossils belongs to Bivalvia class of Mollusca phylum. The vast majority of molluscs live in the seas, a significant amount in the land and a few of them dwell in freshwater. They are divided into seven classes; Aplacophora, Monoplacophopra, Polyplacophora, Scaphopoda, Gastropoda (Snails and slugs), Bivalvia (Mussels and oysters) and Cephalopoda (Octopuses, squid, and cuttlefish) [6].The first four classes live only in the seas and are represented by few species. The bivalves are an important mollusc class, mostly in the sea, and some forms live in freshwater.

There are no protrusions called carina on the shells of freshwater mussels. Most of the mussels living in the sea have these protrusions. In the fossil example in the photograph 2c, the carina, ligament region and umbo part of the sea bivalve are clearly visible. There is no doubt that the fossil, which has carina, is a bivalve species living in the seas (Photograph 2c). These fossils are similar to those of today's living *Flabellipecten* genus.
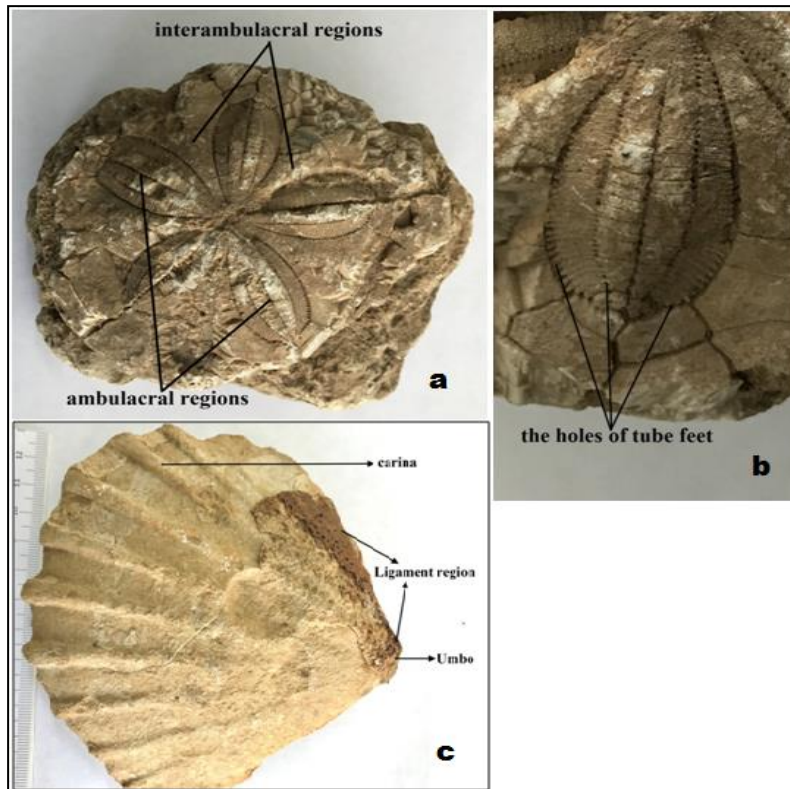
**Photograph 2. a.** Ambulacral and interambulacral regions on a *Clypeaster* fossil, **b.** The holes of tube feet in *Clypeaster* fossil**, c.** Carina, ligament and umbo regions in *Flabellipecten* fossil.

**Table 1.** The systematic of two fossil records, *Flabellipecten* and *Clypeaster*

| **Kingdom:** | Animalia | Animalia |
|---|---|---|
| **Phylum:** | Mollusca | Echinodermata |
| **Class:** | Bivalvia | Echinoidea |
| **Order:** | Pterioida | Clypeasteroida |
| **Family:** | Pectinidae | Clypeasteridae |
| **Genus:** | *Flabellipecten* | *Clypeaster* |

## 4. Conclusions

Turkey, in terms of marine fossils, includes very rich geological plates. For this reason, several researchers have focused on the fossil records of Turkey. In a study on Turkish fossil records, fifteen brachiopod species consisting of two new records (*Paillettiamenaesp. nov*. and *Eodmitriasezgini sp. nov.*) and three crinoid species, have been identified. This fossil assemblage reflects strong affinities with Gondwanan and peri-Gondwanan domains [8]. Anatolia's geological structure is the product of the continents' tectonic movement history because of the location at the intersection of Asia, Europe, and Africa. Turkey's basic rock structure has evolved through the subduction-collision process by combining and accumulating with the Gondwana disposition in the south and the Eurasial disposition in the north, together with the Phanerozoic, Paleo and Neotethyan territories, and the last tectonic movement, which continued until the end of the Middle Miocene period, starting in the Late

Mesozoic, between the Arabian and Eurasial plates [9-12]. From the orogenic records, the Anatolian peninsula witnessed the development of large depressions by the beginning of the Cretaceous period and the Neotethyan suture zones include outcrop plains and valleys between mountains [12, 13]. Devonian units of different litho-types and of different paleogeographic origin are parts of thick Paleozoic sedimentary successions of the Pontides, Taurides and Arabian Plate. In the Taurides of Southern Turkey, it has been distinguished six different tectono-stratigraphic units: Geyikdağ Unit, Aladağ Unit, Bolkardağ Unit, Bozkır Unit, Alanya Unit and Antalya Unit [8, 14].

All along its geological past, Turkey has been located between the two mega-continents: Gondwana to the south and Laurasia to the north. It is generally accepted that numerous continental fragments belonging to one of these mega-continents were drifted off from the main body and amalgamated to the next so that the Anatolian realm is made of several oceanic and continental "terranes" with different geological features. The last main orogenic event, the Alpine orogeny, related to the closure of various Neotethyan branches directly controls the present distribution of these terranes. Southeast Anatolian Zone unit is the northern promontory of the Arabian Platform, which mainly consists of a pan African basement and its Paleozoic-Tertiary cover [15]. Southeast Anatolian Zone is separated from the northerly located Bitlis Unit by an active thrust zone, known as "Southeast Anatolian Fold and Thrust Belt" which can be traced south-eastward for hundreds of km's (Zagros Fold and Thrust Belt). The pre-Cambrian metamorphic basement of Southeast Anatolian Zone is locally observed in Southeast Anatolia [16, 17]. It includes andesitic and rhyolitic lavas and pyroclastics with bimodal chemistry, alternating with fluvial-deltaic type red clastic rocks and mudstones. This rift-related basement complex is transgressively overlain by quartz-arenites that grade into shelf type carbonates and nodular limestone of Middle Cambrian age [15, 18-25]. Southeast Anatolia region covers an area of 120,000 $km^2$ and formed by rocky units from Cambrian to Miocene Eve. The Miocene sequences extend from Ergani and Hani in the north to Harran near the Syrian border in the south. In southern Turkey near Hazro, Hani and Çermik towns of Diyarbakır light and dark beige limestones (Fırat formation) are very rich in fossil records.

Consequently, fossils belonging to Coelenterata, Bryozoa, Brachiopoda, Mollusca, Annelida, Echinodermata, Arthropoda and Hemichordata from invertebrate phyla were found in different parts of Turkey indicated Map 1. The map 1 mostly shows that the fossils belonging to the phyla of Mollusca and Echinodermata are found in the western part of Turkey, outside the region of Diyarbakir. This study reveals that the distribution of Echinodermata and Mollusca fossils in Turkey is also more southeastern. It is of great importance that there are not many studies related to the determinations of the fossils in the southeastern part of Turkey. Probably, with new investigations, marine fossils can be found in many places of Southeast Anatolia region. Approximately 36 million years ago, most of the Southeast Anatolia region was covered with seas. Later on, this sea took its present state about six million years ago by means of withdrawal of the Tethys Sea and shifting of the continents [5].
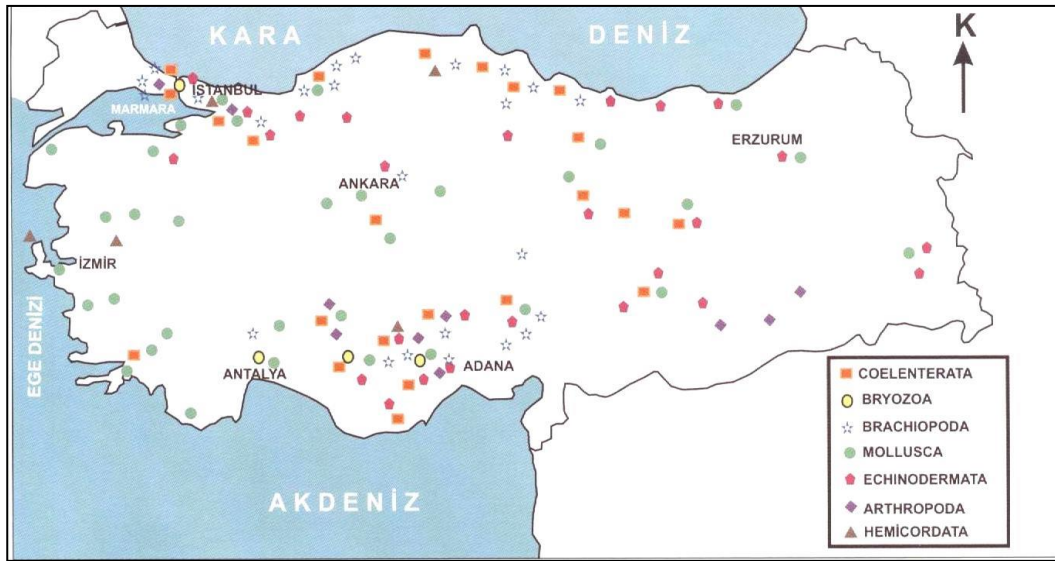
**Map 1.** Distribution of invertebrate fossils according to their phyla in Turkey [4]
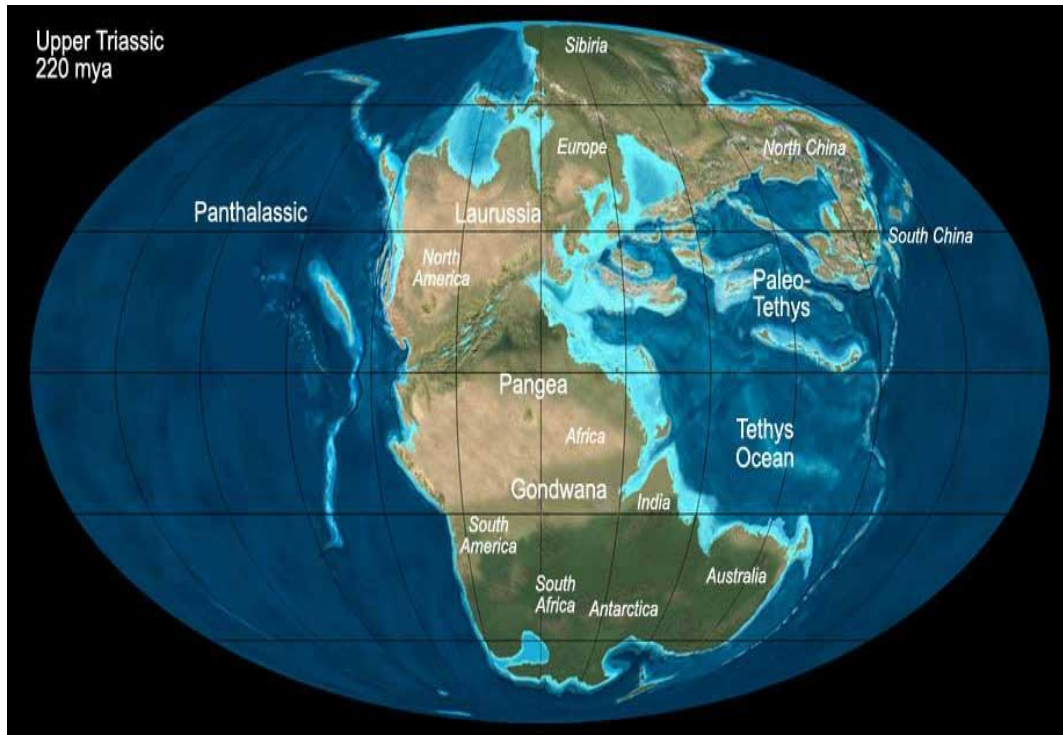


**Map 2.** Earth map: 220 million years ago. On the map, the remains of Anatolia and Laurasia, Gondwana continents have been indicated.(http://www.kerbtier.de/Pages/Themenseiten/enPhylogenie.html)

**References**

[1]    Demirsoy, A., *Basic Rules of Life. General Biology and General Zoology*, Meteksan Inc., Ankara, 2005.

[2]     Cooper, J. D., Miller, R. H., Patterson, J., *A Trip Through Time: Principles of Historical Geology*, Merrill Publishing Company, London, 1986.

[3]     Robetson, A. H. F., Dixon, J. E., ''Introduction: Aspects of the geological evolution of the Eastern Mediterranean'', *Geological Society, London, Special Publications*, 17, 1-74, 1984.

[4]     İnan, N., *Important Invertebrate Fossils of Turkey*, Popular Science Books, TUBITAK, Ankara, 2008.

[5]     Demirsoy, A., *General Zoogeography and Turkey Zoogeography: Animal Geography*, Meteksan Inc., Ankara, 2008.

[6]     Salman, S., *Invertebrate Biology*, Palme Publishing, Ankara, 2006.

[7]     Demirsoy, A., *Inheritance and Evolution*, Meteksan Inc., Ankara, 2008.

[8]     Gourvennec, R., Hoşgör, İ., ''Brachiopods and crinoids from the Middle-Upper Devonian boundary beds in the Darende-Gürün and Van-Zincirkıran areas (Eastern Taurus, Turkey)'', *Bulletin of Geosciences*, 90(3), 577-600, 2015.

[9]     Şengör, A. M. C., Yılmaz, Y., ''Tethyan evolution of Turkey: A plate tectonic approach'', *Tectonophysics*, 75, 181-241, 1981.

[10]    Bozkurt, E., Mittwede, S. K., ''Introduction to the geology of Turkey - a synthesis'', *International Geology Review*, 43, 578-594, 2001.

[11]    Kaymakçı, N., İnceöz, M., Ertepınar, P., ''3D architecture and Neogene evolution of the Malatya Basin: Inferences for the kinematics of the Malatya and Ovacik Fault Zones'', *Turkish Journal Earth Sciences*, 15, 123-154, 2006.

[12]    Özkurt, Ş. Ö., Güleç, E., Erkman, A. C., ''Carnivores from the Late Miocene locality of Hayranlı (Hayranlı, Sivas, Turkey)'', *Turkish Journal of Zoology*, 39, 842-867, 2015.

[13]    Kaymakçi, N., Tectono-stratigraphical evolution of the Çankırı Basin (Central Anatolia, Turkey). Ph. D. thesis, Utrecht University, Utrecht, the Netherlands, 2000.

[14]    Özgül, N., ''Torosların bazı temel jeolojik özellikleri'', *Türkiye Jeoloji Kurumu Bülteni,* 19, 65-78, 1976, (in Turkish).

[15]    Sungurlu, O., ''VI. Bölge kuzeyinin jeolojisi ve petrol imkanları'', *Proceeding of Türkiye İkinci Petrol Kongresi, Tebliğler*, *Ankara, Turkey,* 1974, pp. 85-107, (in Turkish).

[16]    Ketin, İ., ''Güneydoğu Anadolu Paleozoyik teşekküllerinin jeolojik etüdü hakkında rapor (1. kısım: Derik-Bedinan, Penbeğli-Tut ve Hazro bölgesi)'', *TPAO Arama Grubu*, 287, 1-36, 1964, (in Turkish).

[17]    Ketin, İ., ''Güneydoğu Anadolunun Kambriyen teşekkülleri ve bunların Doğu İran Kambriyeni ile mukayesesi'', *Maden Tetkik ve Arama Dergisi*, 66, 75-87, 1966, (in Turkish).

[18]    Schmidt, G. C., ''Stratigraphy of Lower Paleozoic rock units of petroleum distinct V-Turkey'', *Bulletin of Petroleum Administration Publication*, 11, 73-90, 1966.

[19]  Dean, W. T., ''Cambrian Stratigraphy and Trilobites of the Samur Dag Area, South of Hakkari, Southeastern Turkey'', *Turkish Journal Earth Sciences*, 15, 225-257, 2006.

[20]  Demircan, H., Gürsu, S., ''New trace fossils finding in Telbesmi Formation in Southeast Anatolian Autochton Belt (Turkey)'', *Proceeding of IPETGAS*, *Ankara, Turkey*, 2009.

[21]  Göncüoğlu, M. C., Kozlu, H., ''Remarks on the pre-Variscan development in Turkey, Pre-variscan Terrane Analyses of Gondwanean Europa'' *Proceedings* of *Schriften des Staatl Mus Min Geolology Dresden*, *Germany, Vol 9*, 137-138, 1998.

[22]  Göncüoğlu, M. C., Kozlu, H., ''Early Paleozoic evolution of the NW Gondwanaland: Data from southern Turkey and surrounding areas'', *Gondwana Research*, 3, 315-324, 2000.

[23]  Göncüoğlu M. C., Turhan, N., ''Geology of the Bitlis Metamorphic Belt'', *International Symposium on the Geology of the Taurus Belt, MTA Publication*, 237-244, 1984.

[24]  Göncüoğlu, M. C., Turhan, N., ''Rock units and metamorphism of the basement and Lower Paleozoic cover of the Bitlis Metamorphic Complex, SE Turkey, Lower Paleozoic Evolution in Northwest Gondwana'', *Turkish Association Petroleum Geology Special Publications*, 3, 75-81, 1997.

[25]  Göncüoğlu, M. C., Kozlu, H., Dirik, K., ''Pre-Alpine and Alpine terranes in Turkey: Explanatory notes to the terrane map of Turkey'', *Annales Géologiques des Pays Helleniques,* 37, 515-536, 1997.

# MOLLUSCS: THEIR USAGE AS NUTRITION, MEDICINE, APHRODISIAC, COSMETIC, JEWELRY, COWRY, PEARL, ACCESSORY AND SO ON FROM THE HISTORY TO TODAY

*İhsan EKİN[1] \*, Rıdvan ŞEŞEN[2]*

[1]Department of Energy Systems Engineering, Faculty of Engineering, Şırnak University, Şırnak, Turkey
[2]Department of Biology, Faculty of Science, Dicle University, Diyarbakır, Turkey

\*Correspondence: e-mail: ekinihsan@gmail.com

**Abstract:***The present study has evaluated the usage and properties of the mollusca phylum from the history to today. Many types of molluscs are eaten worldwide, either cooked or raw due to their rich nutritional value. Furthermore, they are used as pearl, cowry and accessory materials, for tools like household dishes, cooking pots and utensils such as a spoon, cutlery, scoops, spatulas, etc. Some of them are destructive and caused ecological damage, some serve as intermediate hosts for human parasites; some can cause damage to crops. Mollusc meat is known to be highly nutritious and salutary owing to its high content of essential amino acids, proteins, fatty acids, vitamins, and minerals. In addition, some of the bioactive compounds including antiviral, antimicrobial, antiprotozoal, antifungal, antihelminthic and anticancer products are producing by molluscs as medicines. The largest edible snail is African land snail Achatina achatina mostly consumed by African people. Molluscs were very prominent dishes during the Roman Empire due to their aphrodisiac effect. Some mollusc species include zinc and essential amino acids which keeping up body energy and boost sex drive as an aphrodisiac, arrange immune system and makes bones stronger. Pearls are highly esteemed bivalve products containing nacreous deposit composed of 82 - 86% calcium carbonate (aragonite crystals), 10-14% organic substance conchiolin and 2-4% water. Cowry is amarine snail from genus Cypraea dwelling on mostly in coastal waters of the Indian and Pacific oceans and used instead of money. Money cowry (Cypraea moneta), a 2.5cm yellow species, has served as currency in Africa.*
Keywords: *Molluscs, Nutrition, Medicine, Cowry, Pearls,*

## 1. Introduction

Phylum Mollusca is divided into seven classes; Aplacophora, Polyplacophora, Monoplacophora, Gastropoda (Prosobanchia, Opisthobranchia, Pulmonata), Bivalvia (Protobranchia, Lamellibranchia, Septibranchia), Scaphopoda (tusk shells) and Cephalopoda (Nautilodea, Ammonoidea, Coleoidea). This phylum is the second largest phylum in numbers of species containing

over 128.000 described species. They are ecologically widespread, dwelling on marine, freshwater, terrestrial habitats, as well as gastropods, are successfully adapted to land. They can be great variety in body size, roughly from 1 mm to 18 m. Many sorts of molluscs such as clams, scallops, snails, squids, whelks, cockles, mussels, octopus, oysters, periwinkles, and winkles are consumed by humans from historic times to today. Mankind has been deliberately culturing molluscs as food for a long time and the earliest known records of someone farming molluscs for food come from Roman Empire.

## 2. Usage Areas of Molluscs and Their Benefits to Mankind
### 2.1. Nutritional contribution of molluscs for human diets

Human beings have eaten snails for thousands of years and nowadays snails are considered to be common food consumed by millions of people worldwide, particularly in European countries [1, 2]. Additionally, the cephalopods which include the cuttlefishes, squids and the octopus are generally operated for food fishes in most part of the world. In most of the countries, oysters and mussels are used in the dishes and eaten as an aperitif meal. The largest edible land snail is the giant African land snail *Achatina achatina* mostly consumed by African people. It can weigh up to 900 g and measure up to 40 cm from snout to tail. In Turkey, *Helix aspersa, Theba pisana, Eobania vermiculata, Cantareus apertus, Helix asemnis, Helix cincta*and *Helix lucorum* are commercially important edible snails and mostly exported to France, Greece, Germany, Italy and Spain [3-5]. Snail meat (escargot) is not only tasty but also has several advantages over others: quite a low lipid rate and calorie values versus rich mineral, essential amino acid and fatty acid content, especially polyunsaturated fatty acids (PUFA). With higher omega-3 fatty acid content, snail meat is found being a factor affecting higher lifespan and lower cancer rate in most of the countries. Calcium, magnesium, zinc, copper, manganese, cobalt, and iodine are the predominant minerals of molluscs' flesh [3-5].

### 2.2. Products and metabolites obtained from molluscs as medicines

Molluscs used directly as a food source may also contribute to the prevention of disease by providing essential nutrients, as well as immuno-stimulatory compounds and other secondary metabolites with direct biological activity [6]. Most of the molluscs are the source of lipid bioactive compounds offering a variety of nutraceutical and pharmaceutical applications [6]. Among them, the PUFA omega-3 fatty acids such as eicosapentaenoic acid, (C20:5ω3), and docosahexaenoic acid (C22:6ω3) are known for their beneficial effects on human health [4, 5, 7]. These PUFA ω3 fatty acids are widely known for their capacities on cardio protection. They reduce triacylglycerol and cholesterol levels and have anti-inflammatory and anticancer effects. Numerous experiments on these animals confirmed the cancer preventive properties of PUFA ω3 fatty acids from marine sources [7, 8].

The deadly venoms of some Cone shells (Conidae) are today being used to help victims of strokes and heart disease, and to produce a revolutionary new drug for chronic pain control called Ziconotide. An extract from the hard clam *Mercenaria mercenaria L.* is a strong growth inhibitor of cancers in mice. The drug is called Mercenine. Ground and processed oyster shells are used as calcium supplements both for humans and animals. Paolin, a drug made of abalone juice, is an effective inhibitor of penicillin-resistant strains of bacteria such as *Staphylococcus aureus*, *Streptococcus pyogenes*, *Salmonella typhus*. Oyster juice has been found to have antiviral effects and may be made into a drug eventually [9]. The venom of Cone snails used for hunting their prey can be dangerous, even lethal for humans. The venom is a neurotoxin and being studied for use in medicine.

Since its toxin paralyzes the prey, it is being used to help patients with chronic pain, and it also shows promise in treating epilepsy in the future [9].

### 2.3. Aphrodisiac effect of bivalves

The interactions between man and snails have been recognized from the earliest times. These interactions became very prominent during the height of the Roman Empire when it was a common practice to eat snails in the courts of the Emperor where they are used as an aphrodisiac [10]. The researchers have analyzed bivalve molluscs, particularly oysters and realized that they are rich in rare amino acids which trigger sex hormones level increasing. Most of the edible oysters are known as aphrodisiac sources. *Aplysia dactylomela*, a species of local sea slug is also aphrodisiac effect in the human body [11]. In some traditional place, people consume *A. dactylomela* raw to warm up their bodies before going to the sea [12]. Furthermore, it is believed that *A. dactylomela* contains a high level of steroids hormones [13]. On the other hand, oysters are rich in zinc, which is one of the essential minerals and might have been associated with improving sexual potential in men. Adequate zinc is needed for sperm production and hormone metabolism. Oyster efficacy is yet to be scientifically validated before claiming that oysters have the aphrodisiac effect due to their pharmacological properties [14].

### 2.4. Cosmetic industry uses molluscs for products

Snail and slug have been used sporadically as skin treatments since the time of the Ancient Greeks. Hippocrates reportedly recommended the use of crushed snails to relieve inflamed skin and some 20 years ago as well as the potential of snail slime was noted by Chilean snail farmers who found that skin lesions healed quickly, with no scars, when they handled snails for the French food market. This investigation resulted in the production of "Elicina", a Chilean snail slime-based product [15]. In 2010, Aqua Cell Renew Snail Cream, claiming that its 70% snail extract, soothes regenerates and heals skin. Snail slime based products are claimed to be the new miracle face-fixer in the U.S where they are used to treat acne, reduce pigmentation and scarring, and combat wrinkles [15]. Slugs are used in Italy to treat dermatological conditions. Mucus collected from a slug is rubbed onto the skin to treat dermatitis, inflammations, acne and to promote wound healing and used for the treatment of warts. Mucus from a live slug is first rubbed onto the wart and then the slug is hung out in the sunshine to dry out and die. It is believed that once the slug has dried up, the wart disappeared [16].

### 2.5. Pearls as precious jewelry obtained from molluscs

Conchifera is the subphylum of molluscs that produce pearls. Although none of the molluscs within the Conchifera subphylum can produce pearl-like formations, actually Bivalvia class of mollusc is the outstanding group for the formation of pearls. Meanwhile, some gastropods and cephalopods species also produce pearls. Although the shell of each mollusc is significant for identification of pearl formation, it is actually the inner soft body (mantle) of the mollusc that scientifically defines the species for the pearl. Black pearls are very expensive and come from *Pinctada margaratifera* showing a wide range of color and luster, which are the most important characteristics determining their commercial value. This variation is probably to be influenced by both environmental and genetic factors. The latter may depend on the recipient oyster, but professional grafters commonly consider that the color and luster of pearl is often related to the phenotypic properties of donor oyster [17].

Pearls are highly esteemed bivalve product containing nacreous deposit composed of 82 - 86% calcium carbonate (aragonite crystals), 10-14% organic substance conchiolin and 2-4% water. They are produced when a tiny particle of sand or grit is trapped between the mantle and the shell; the animal forms a protective cover around the irritant. The substance used to form this covering, the pearl, is made from the iridescent material that lines the interior of the shell. It is called nacre or aragonite. Some of the pearls used as valuable jewelry are made by natural pearl oysters and freshwater mussels, however, most of the ones traditionally sold are cultured and not wild [18].

## 2.6. Ancient money cowry and accessories from mollusc shells

Cowry comes from genus *Cypraea,* family Cypraeidaea and has hard humped thick, colorful and glossy shell. It occurs dominantly in coastal waters of the Indian and Pacific oceans. The 10 cm golden cowry (*Cypraea aurantium*) was traditionally worn by royalty in Pacific Islands, and the money cowry (*Cypraea moneta*), a 2.5 cm yellow species, has served as currency in Africa and elsewhere [19]. Cowry is called the kabttaj (Maldives), kauri (Bengal), kaudi (Hindi), kaoli (Chinese), kavari (Martha) and cowry (English) and it is believed that it has been the first universal money. It has lasted longer than any other in human history so far. Prior to being globally distributed on a large scale, it was a scare and valuable item. Imitations of this shell have been made of wood, stone, jade, other semi-precious stones, bone, bronze and even silver and gold. Marco Polo told of the cowry being used as currency in many regions across Eurasia. Today, cowries are still used as currency in Ethiopia and other remote corners of Africa [20].

Additionally, mollusc shells are sometimes used as ornaments in homes and workplaces being decorative items as well as valuable habiliments in tribes by ladies and men. Furthermore, they are used as accessory materials, for tools like household dishes, cooking pots and utensils such as a spoon, cutlery, scoops, spatulas, etc. Some shells are often collected because of their great beauty. The more rare and beautiful the mollusc, the more coveted is its shell. Unfortunately, collectors usually kill these species so as to get its shell. This has resulted in many of the rare and unusual mollusc's species becoming endangered.

## 2.7. Byssus from bivalve processed for valuable thread and fabric

Mussels attach to the substratum by means of a byssus, which is an extracellular, collagen structure secreted by the foot. It is believed to be the finest fabric known to Egypt, Greece, and Rome. If treated properly with lemon juice and spices, the remarkable material shines when exposed to the sun. It is also incredibly light, for this reason, the wearer cannot even feel it touching the skin. It is said to be as thin as a spider web, resistant to water, acids, and alcohols. Byssus fibers produced by mussels are tough biopolymers composed mainly of proteins and water. These natural biopolymer fibers have been intensively studied owing to their mechanical and adhesive properties. The extraordinary strength, unmatched toughness, and extensibility of byssus fibers allow mussels to withstand the large and repetitive forces produced by waving and crashing. They are composed of three collagen proteins that make up the bulk of the thread core. Their toughness is considered six times greater than that of the human tendon collagen and comparable with that of Kevlar and carbon fibers [21]. Nowadays, rare fabric production from byssus in some places is present, however, the cost of the fabric and thread are very expensive.

## 2.8. Cleaning the water for better environment via bivalves

Each oyster filters about 30 to 50 gallons of water a day. Think of how much water a whole bed of those awesome bivalves is cleaning, which makes these not only tasty creatures but good for the environment ones as well. In many lakes, rivers, seas and water pools, the bivalves filter the water and make them as a clean environment for other living creatures. Mussels and clams are clean up the polluted waters by microorganisms. Bivalves serve as tiny water filtration systems, constantly sieving the water around them in their hunt for a meal of bacteria or microscopic algae known as phytoplankton. As they filter water, their tissues absorb some of the chemicals and pathogens that are things like protozoan, herbicides, pharmaceuticals and flame retardants [22].

## 2.9. Qualified dyes, ink and glues obtained from molluscs

In ancient times, dyes were made from various molluscs. The most famous was from *Bolinus brandaris*, a gastropod, from which Tyrian or imperial purple was obtained. Its common name is the purple dye Murex. Purple was indeed extracted from the marine gastropod mollusc "murex", which has a spiny shell and lives near the coasts of Mediterranean Sea, length up to 8 cm for the largest species. To extract the dye, shells were broken and the molluscs were macerated in basins. The obtained dye could vary from pink to violet through crimson by using different sun-drying times. Because of resistance to the dye and difficulty in harvesting the animal, purple fabrics were expensive and highly estimated. They were only used for the cloth of noblemen, kings, priests, and judges. The purple color, similar to blood, became a sign of temporal and spiritual power. Under the Roman Empire, the chief commanders of the armies wore the "paludamentum", a purple coat. However, nowadays, the main component of the dye can easily be obtained through chemical synthesis [23].

Recently, the threads that some mussels (Mytilidae) use to attach themselves to rocks, piers, and other hard surfaces are being tested as possible glue in surgery [9]. Additionally, many cephalopod molluscs living in low-light or dark conditions, including the deep sea produce ink, actually for hunting and protection. The ink sac is present at hatching, so even at a small size and young age. Cephalopod ink is composed of secretions from two glands. The ink sac with its ink gland produces a black ink containing melanin, and most of the cephalopod ink comes from this part. A second organ, the funnel organ, is a mucus-producing gland that is much more poorly studied [24].

## 2.10. Inspiration from molluscs for surgical studies

Scallops have rings of bright blue eyes around the edges of their shells, though they can actually only detect light and dark. However, their eyes have inspired research into various ways of seeing and optical devices Since the axons of the nerve cell of cephalopods are larger than other creatures, many experiments related to nervous system disorders are conducted on these axons. Side effects of some medicines are determined by trying on mollusc species and then their usage is presented and controlled.

The new adhesive combines the positively charged polymers found in slug go with hydrogels, forming a bond, and the resulting substance is a strong adhesive that can stick to skin, cartilage, arteries, and other types of living tissues without the issues that current medical glues have. Currently, used products can be easily dislodged, can be toxic to certain tissues, and may become brittle. The new glue shows greater strength than the current generation of surgical adhesives, and crucially, (can stretch to 14 times its original size before failing), and sticks slowly over a period of time, which

facilitates easy repositioning if needed. Also, the new product demonstrated low toxicity to living tissue. The adhesive is not commercially available yet but shows the incredible potential in something as insignificant as a garden slug [25].

**3. Conclusion**

Molluscs are extremely important members of many ecological communities, ranging in distribution from terrestrial mountain tops to the hot vents and cold seeps of the deep sea. They can range in size from twenty-meter long giant squid to microscopic aplacophorans, a millimeter or less in length, that live between sand grains. Besides having tasty nutritional parts, molluscs often have valuable hard parts as shells and pearls. These creatures have been important to humans throughout history as a source of nutrition, biomolecules, secondary metabolites, cosmetics, medicine, jewelry, tools, pearls, currency, musical instruments, fabric and etc. In recent times, we have heard alarming news about these creatures. If serious measures related to their protection are not taken, a majority of these creatures can be exhausted in the future.

**References**

[1] Murphy, B., *Breeding and Growing Snails Commercially in Australia*, RIRDC-Rural Industries Research Development Corporation, Kingston, 2001.

[2] Jess, S., Marks, R. J., ''Effect of temperature and photoperiod on growth and reproduction of *Helix aspersa var. maxima*'', *Journal of Agricultural Science*, 130, 367-372, 1998.

[3] Yıldırım, M. Z., Kebapçı, Ü., ''Slugs (Gastropoda: Pulmonata) of the Lakes Region (Göller Bölgesi) in Turkey'', *Turkish Journal of Zoology*, 28, 155-160, 2004.

[4] Ekin, İ., Başhan, M., ''Fatty acid composition of selected tissues of *Unio elongatulus* (Bourguignat, 1860) (Mollusca: Bivalvia) collected from Tigris River, Turkey'', *Turkish Journal of Fisheries and Aquatic Sciences*, 10, 445-451, 2010.

[5] Ekin, İ., Bashan, M., Şeşen, R., ''Possible seasonal variation of the fatty acid composition from *Melanopsis praemorsa* (L., 1758) (Gastropoda: Prosobranchia), from southeast Anatolia, Turkey'', *Turkish Journal of Biology,* 35, 203-213, 2011.

[6] Benkendorff, K., ''Molluscan biological and chemical diversity: Secondary metabolites and medicinal resources produced by marine molluscs'', *Biological Review*, 85, 757-775, 2010.

[7] Simopoulos, A. P., ''The importance of the omega-6 / omega-3 fatty acid ratio in cardiovascular disease and other chronic diseases'', *Experimental Biology and Medicine*, 233, 674-688, 2008.

[8] Wendel, M., Heller, A. R., ''Anticancer actions of omega-3 fatty acids - Current state and future perspectives'', *Anticancer Agents in Medicinal Chemistry*, 9, 457-470, 2009.

[9] Lakshmi, S. A., ''Wonder molluscs and their utilities'', *International Journal of Pharmaceutical Sciences Review and Research*, 6(2), 30-33, 2011.

[10] Taylor, J. W., Monograph of the land and fresh water molluscs of the British 1sles, in: *Structural and General* (Ed. Taylor and Bros), p. 454, United Kingdom, Leeds, 1900.

[11] Ridzwan, B. H., Hanani, M., Siti Norshuhada, M., Farah Hanis, Z., Aileen, T. S. H., ''Screening for aphrodisiac property in local oyster of *Crassostrea iredalei*'', *Journal of World Applied Science*, 26(12), 1546-1551, 2013.

[12] Hashim, R., *Marine food resources from coastal area of Sabah,* Selangor, Dewan Bahasa and Pustaka, Malay, 1993.

[13] Wang, C., Croll, R. P., ''Effects of sex steroids on spawning in the sea scallop, *Placopecten magellanicus*'', *Aquaculture*, 256, 423-432, 2006.

[14] ***, Aphrodisiacs, http://www.loveologyuniversity.com /lupages/aphrodisiacs.aspx

[15] ***, Mail online*,* http://www.dailymail.co.uk/femail/article-2216457/Snail-slime-hailed-latest-beauty-wonder-product-promising-clear-acne-reduce-scarring-beat-wrinkles.html.

[16] Quave, C. L., Pieroni, A., Bennett, B. C., ''Dermatological remedies in the traditional pharmacopoeia of Vulture-Alto Brandano, inland southern Italy'', *Journal of Ethnobiology and Ethnomedicine*, 4, 5. 2008.

[17] Wada, K.T., Komaru, A., ''Color and weight of pearls produced by grafting the mantle tissue from a selected population for white shell color of the Japanese pearl oyster *Pinctada fucata martensii* (Dunker)'', *Aquaculture*, 142, 25-32, 1996.

[18] ***, Pearls and other organic gems, https://nature.berkeley.edu/classes/eps2//wisc/oLect17.html

[19] ***, Encyclopaedia Britannica, Cowries, https://www.britannica.com/animal/cowrie

[20] Yang, B., ''The rise and fall of cowrie shells: The Asian Story'', *Journal of World History,* 22(1), 1-25, 2011.

[21] Waite, J. H., ''Adhesion à la Moule'', *Integrative and Comparative Biology*, 42, 1172-1180, 2002.

[22] ***, Seeker, Feed your curiosity, https://www.seeker.com/mussels-and-clams-can-clean-up-polluted-water-1768972732.html

[23] ***, Ancient dyes, http://www.crwflags.com/fotw/flags/xf-dye.html

[24] Bush, S. L., Robison, B. H., ''Ink utilization by mesopelagic squid'', *Marine Biology*, 152, 485-494, 2007.

[25] ***, Life mirror, https://lifemirror.net/2017/07/27/researchers-develop-new-surgical-adhesive-inspired-by-slug-secretions/

# PRODUCTION POTENTIAL OF FRUITS GROWN ON KARS PROVINCE

*Mikdat Şimşek\*[1]*

[1]Dicle University, Faculty of Agriculture, Diyarbakir, TURKEY

\*Corresponding author; mikdat.simsek@dicle.edu.tr

**Abstract:** *In every province of Turkey more or less fruit species and varieties are grown. One of the most important factors limiting the fruit growing of Kars province of Eastern Turkey. Four fruit species are grown in Kars  and their name are walnut, apple, plum and apricot. Considering the total fruit production of Kars districts, Kağızman and Sarıkamış are  6.841 and 1.085  tons of fruit productions, respectively. No fruit production has the other districts. One of the most important reasons for not cultivating fruit species and varieties in the other districts of Kars province is the ecological conditions called climate and soil properties. In this study, through presenting the existing status of the fruit production potential of Kars province, it was aimed to increase the awareness and set light to decision makers.*

Key words*: Kars, Fruit production, development opportunities.*

## 1. Introduction

The production of plants is healthier supply of raw materials to the industry and some crops are subject to export is an important production activity. Fruits have effects on human health [1]. Consumption of fruits and vegetables has been strongly associated with reduced risk of cardiovascular disease, cancer, diabetes and age-related functional decline [2]. Therefore, production of a lot of fruits and many other plants is of great importance in the world  because of human nutrition, raw material supply for industry and foreign trade [3, 4].

Anatolia, as a country possessing different climates and lying in a passageway between the gene centers named the Caucasian and the Mediterranean, bears many fruit species [5]. In this context, some of the fruits known as apricot, walnut and apple have been traditionally and/or  modernly produced and consumed for centuries.

Turkey has a quite large potential regarding fruit species and production in the world [6]. and has favourable ecological conditions for growing many fruit species and cultivars [7]. In this context, Anatolia is a gene centre for many fruit species such as pistachios, figs, hazelnuts, almonds, apricots, walnuts, pomegranates and apples.  Many fruit species were grown in Anatoliaa few thousand years ago [8]. However, Kars province has four fruit species grown generally, which are walnut, apple, plum

and apricot [9]. The greatest reason for the small number of fruit species that grow and produce stems from the ecological conditions of this province.

Kars province has a severe high plateau climate. This province is under the influence of the high-pressure center of Siberia. Winter lasts seven months. Snow is high. Snow is close to 50 days in the sun and the ground remains covered with snow for 100 days. The spring and autumn seasons are short enough to be tried. The annual amount of rainfall is 528 mm in some places and 252 mm in some places [10].

Kars province is mentioned with its famous Beylerbeyi palace (Fig. 1) and Sarıkamış ski resort (Fig. 2) in the world. In this study, through presenting the existing status of the fruit production potential of Kars province, it was aimed to increase the awareness and set light to decision makers in future plans for making use of the existing fruit potential.
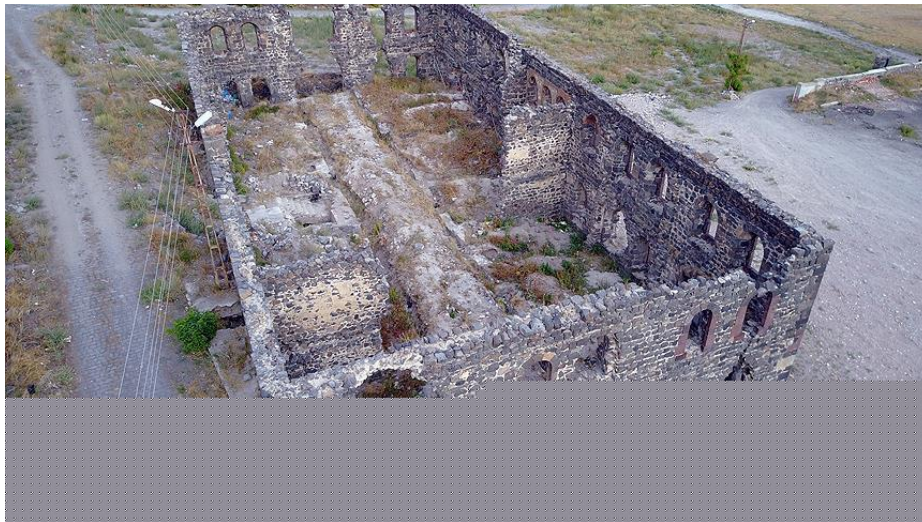


**Fig. 1.** Beylerbeyi Palace [11]



**Fig. 2.** Sarıkamış Ski Resort [12]

## 2. Fruit Production Potential of Kars Province

Kars province of Turkey map and the districts's map of this province were given Fig. 3.and Fig. 4, respectively. Our country have 237.625.723 decares of area of agricultural land and 33.292.166 decares of the area for fruits and the beverage-spice [9]. According to the year of 2016, Kars province has 7.926 tons of fruit potential production, 112.006 of number of fruitful trees, 33.667 of number of unfruitful trees and 145.673 of total number of trees [9] (Table 1). The fruits's name grown in Kars are apple, walnut, pear, plum and apricot. Although fruit production have Kağızman and Eleşkirt districts, No fruit production has the others. Therefore, this province is suitable for the cultivation of some fruit species and varieties.



**Fig. 3.** Kars Map in Turkey [13]



**Fig. 4.** Kars Districts's Map (14)

**Table 1.** Kars province's fruit production ([9]

| District | Area covered by bulk fruit (decare) | Production (ton) | Number of fruitful trees | Number of unfruitful trees | Total number of trees | District |
|---|---|---|---|---|---|---|
| Walnut | 684 | 82 | 57 | 1.440 | 6.705 | 8.145 |
| Apple | 1.816 | 1.330 | 69 | 19.271 | 5.787 | 25.058 |
| Plum | 6 | 1 | 67 | 15 | 10 | 25 |
| Apricot | 6.382 | 6.513 | 71 | 91.280 | 21.165 | 112.445 |
| TOTAL | 8.888 | 7.926 | | 112.006 | 33.667 | 145.673 |

## 3. Fruit Potential Production of Kağızman District

Kağızman district has 6.841 tons of fruit production, 101.401 of number of fruitful trees, 29.107 of number of unfruitful trees and 130.508 of total number of trees. The highest and lowest fruit production in Sarıkamış district were obtained from apricot with 6.321 tons and from walnut with 57 tons, respectively (Table 2).   In addition, this district has 463 tons of apple [9]. According to these information, Kağızman district is suitable for the cultivation of apricot, apple and walnut species and varieties.

## 4. Fruit Potential Production of Sarıkamış District

Sarıkamış district has 1.085 tons of fruit production, 10.605 of number of fruitful trees, 4.560 of number of unfruitful trees and 15.165 of total number of trees. The highest and lowest fruit production in Sarıkamış district were obtained from apple with 867 tons and from plum with 1 ton, respectively (Table 2).   In addition, this district has 192 tons of apricot and 25 tons of walnut [9]. According to these information, Sarıkamış district is suitable for the cultivation of apricot, apple, walnut and plum species and varieties.

## 5. Fruit production potential of the other districts

Kars province has eight districts named  Akyaka, Arpaçay, Digor, Kağızman, Sarıkamış, Selim, Susuz and Center [15]. Although fruit production have Kağızman and Sarıkamış districts, No fruit production  according to TSI [9] has the others. Therefore, the development of fruit production in Sarıkamış and Kağızman districts will give more beneficial results. But, It should be applied to studies of adaptation to various fruit species in some microclimatic areas, taking into consideration the ecological characteristics of other districts.

**Table 2.** Fruit potential production of Kars districts [9]

| District and fruit name | Area covered by bulk fruit (ha) | Production (ton) | Average yield per tree (kg) | Number of fruitful trees | Number of unfruitful trees | Total number of trees |
|---|---|---|---|---|---|---|
| Walnut | 650 | 57 | 50 | 1.150 | 6.555 | 7.705 |
| Apple | 923 | 463 | 43 | 10.671 | 2.387 | 13.058 |
| Apricot | 6.200 | 6.321 | 71 | 89.580 | 20.165 | 109.745 |
| **KAĞIZMAN** | **7773** | **6.841** | | **101.401** | **29.107** | **130.508** |
| Walnut | 34 | 25 | 86 | 290 | 150 | 440 |
| Almond | 893 | 867 | 101 | 8.600 | 3.400 | 12.000 |
| Plum | 6 | 1 | 67 | 15 | 10 | 25 |
| Apricot | 182 | 192 | 113 | 1.700 | 1.000 | 2.700 |
| **SARIKAMIŞ** | **1.115** | **1.085** | **367** | **10.605** | **4.560** | **15.165** |

## 6. Development Opportunities of Fruit Production Potential of Kars Province

One of the most important factors limiting the fruit growing of Kars province of East Anatolia Region of Turkey are the ecological conditions. However, the fruit species's grown in this province are apple, plum, apricot and walnut. It is possible to increase the production of these fruit species. It should be applied to studies of adaptation to various fruit species in some microclimatic areas of the ecological characteristics of other districts. At that time, fruit production in Kars province could be further improved.

## References

[1] Simsek, M., Gulsoy, E.A., "Research on pomegranate (*Punica granatum* L.) productıon potentıal of Southeastern Anatolıa Regıon", *Iğdır University Journal of Institute Science & Technology*, 7, 131-141, 2017.

[2] Liu, H.I., "Health benefits of fruit and vegetables are from additive and synergistic combinations of phytochemicals", *The American Journal of Clinical Nutrition*, 78, 517S–520S, 2003.

[3] Simsek, M., Gulsıy, M., "The important in terms of humanhHealth of the walnut and the fatty acids and some studies on this subject", *Iğdır University Journal of Institute Science & Technology*, 6, 9-15, 2016.

[4] Simsek, M., Kızmaz, V., "Determination of chemical and mineral compositions of promising almond (*Prunus amygdalus* L.) genotypes from Beyazsu (Mardin) Region", *International Journal of Agriculture and Wildlife Science*, 3, 6-11, 2017.

[5] ***, Present Status and Future Prospects of Underutilized Fruit Production in Turkey, http://agris.fao.org/agris-search/search.do?recordID=QC9665645

[6] Dizdaroğlu, T., Economic Evaluation of Peach, Apricot and Plum Cultivation in İzmir's Menemen Village, Ph. D. thesis, Ege University, İzmir, 1985.

[7] Simsek, M., Kara, A., "Diyarbakir Fruit Growing Potential An Overview", *International Diyarbakir Semposium 2-5 October, Diyarbakır-Turkey, 2016.*

[8] Gercekcioglu, R., Bilgener, S., Soylu, A., General Orcharding (Principles of Fruit Growing), NOBEL Academic Publishing, Improved 4th Edition, Istanbul, p.498, 2014.

[9] ***, Turkish Statistical Institute, www.tuik.gov.tr

[10] ***, Kars İklimi, http://www.cografya.gen.tr/tr/kars/iklim.html

[11]***, Kars Beylerbeyi Sarayı, https://www.google.com.tr/search?safe=active&biw=1366&bih=637&tbm=isch&sa=1&ei=GgoYWqbRMcPPwQKiyY-gAg&q=Kars+Beylerbeyi+Saray%C4%B1&oq=Kars+Beylerbeyi+Saray%C4%B1&gs_l=psy-ab.3..0.19815.19815.0.21282.1.1.0.0.0.0.131.131.0j1.1.0....0...1c.1.64.psy-ab..0.1.130....0.gOJpzIZcXBE#imgrc=VLpprR0Stw2WCM:

[12]***, Sarıkamış Kayak Merkezi, https://www.google.com.tr/search?q=Sar%C4%B1kam%C4%B1%C5%9F+Kayak+Merkezi&safe=active&source=lnms&tbm=isch&sa=X&ved=0ahUKEwjMr4DPk9fXAhWCZFAKHTBGAxAQ_AUICigB&biw=1366&bih=637#imgrc=l0PIlOsmOWyMnM:

[13] ***, Kars Map in Turkey, https://www.google.com.tr/maps/@39.0688728,35.8820443,1016084m/data=!3m1!1e3?hl=tr

[14] ***, Kars districts's map, https://www.google.com.tr/search?q=Kars+il%C3%A7eleri&safe=active&source=lnms&tbm=isch&sa=X&ved=0ahUKEwik0YKcztbXAhXEIlAKHVvoAcwQ_AUICygC&biw=1366&bih=637#imgrc=XUOk_Is-17KkMM:

[15] ***, Kars İlinin İlçeleri, https://www.google.com.tr/search?safe=active&ei=dzgYWoKjLsLdwALh9omwCQ&q=Kars+il%C3%A7eleri&oq=Kars+il%C3%A7eleri&gs_l=psy-ab.3..0l10.5922.11128.0.11494.16.12.0.4.4.0.129.1475.0j12.12.0....0...1c.1.64.psy-ab..0.16.1498...0i131i67k1j0i131k1j0i67k1.0.s1gDkHrwYq0